EPITAXIAL CRYSTAL GROWTH BY SPUTTER DEPOSITION: APPLICATIONS TO SEMICONDUCTORS. PART 2

Author: **J. E. Greene**
Department of Metallurgy,
Coordinated Science Laboratory, and
Materials Research Laboratory
University of Illinois
Urbana, Illinois

TABLE OF CONTENTS

V. CRYSTAL GROWTH OF EPITAXIAL SEMICONDUCTOR FILMS BY SPUTTER DEPOSITION: EXPERIMENTAL RESULTS

Sections I through IV, presented in Part 1 of this review, included discussions on experimental techniques, the physics of ion/surface interactions, and ion bombardment effects on film nucleation and growth kinetics. In this section, the literature on the growth of epitaxial semiconductor films is reviewed in detail in this section. The discussion is divided into separate subsections on elemental semiconductors, III-V, II-VI, IV-VI, "other" semiconductors, and metastable semiconducting alloys. In each case, an attempt was made to provide a critical analysis of the present understanding and state of the art. Early work on sputter deposition is described in a series of general review articles by Francombe[223-225] as well as in more recent reviews by Greene[226] and Greene and Eltoukhy[227] directed specifically towards semiconductors.

Figure 23 summarizes in the form of a schematic pseudophase diagram the general results of vapor phase crystal growth studies carried out as a function of growth temperature T_s and deposition rate R. The phase fields in this diagram represent the crystalline state of the film: amorphous, polycrystalline, or single crystal. The phase boundaries are actually not sharp as shown and, in fact, their placement is somewhat subjective depending on the criteria adopted for interpreting diffraction data. Nevertheless, the general features of the diagram are correct. The crystalline quality of an as-deposited film in a clean system increases at higher T_s (provided that decomposition does not occur) and lower R values. In addition, for a given film/substrate combination, the transition between amorphous and polycrystalline films is a strong function of the growth temperature and, generally, only weakly dependent on deposition rate. However, an accurate measure of critical growth temperatures is difficult to obtain since initially deposited amorphous layers may transform to the crystalline state due to annealing

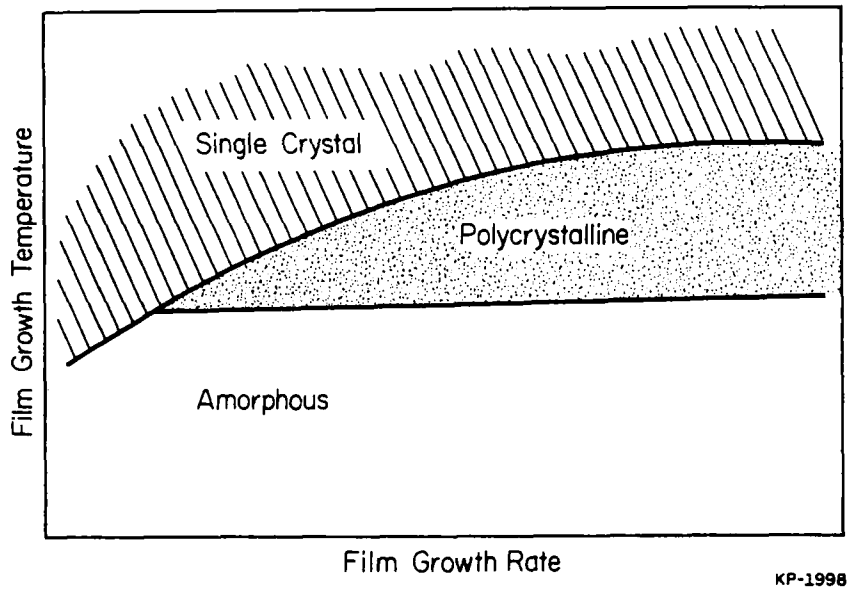

FIGURE 23. A schematic phase map of the crystallinity of as-deposited metal and semiconducting films as function of growth rate and temperature.

during the deposition of subsequent layers. The enthalpy of amorphous to crystalline transformations is typically on the order of 10 to 100 meV. Within the polycrystalline phase field, increasing T_s, or decreasing R results in an increase in the preferred orientation of the deposited film.

The polycrystalline to single crystal transition depends strongly on both T_s and R through nucleation kinetics, and single crystal films grown near the transition region may still contain substantial densities of mechanical defects such as twins and stacking faults. At very low values of R, it is sometimes possible to observe direct transitions from amorphous to single crystalline structures with no intermediate polycrystalline phase. As discussed in Section IV.B.1, both the amorphous to polycrystalline and the polycrystalline to single crystal transition temperatures can be decreased for a given R by the use of low energy ion irradiation during deposition.

A. Elemental Semiconductors

1. Germanium

Most of the early work on the sputter growth of epitaxial semiconductors was carried out on Ge.[228-232] Krikorian and Sneed[228,232] and Krikorian[229] investigated the effects of film growth rate, growth temperature, and the background system pressure on the epitaxial growth of sputtered Ge on (100) and (111) oriented Ge substrates as well as on cleaved (111) CaF_2. The experiments were carried out in a dc system with a base pressure of $< 1 \times 10^{-6}$ Torr (1.3×10^{-4} Pa) using target voltages V_T and Ar sputtering pressures P_{Ar} in the range from -2 to -5 kV and 8 to 65 mTorr (1 to 8.6 Pa), respectively. Figure 24 shows typical results for the sputter growth of Ge at $V_T = -3$ KV on (111) Ge. The growth rate shown in Figure 24 was varied by changing P_{Ar}.

Kahn[233] studied the effects of background gas contamination and substrate preparation on the homoepitaxial growth of Ge on (111) Ge in an UHV (2×10^{-10} Torr, 2.7×10^{-8} Pa) dc sputtering system. The films were grown at Ar pressures of 10 to 100 mTorr (1.3 to 13.3 Pa) with a target voltage of -2 kV. High energy and low energy

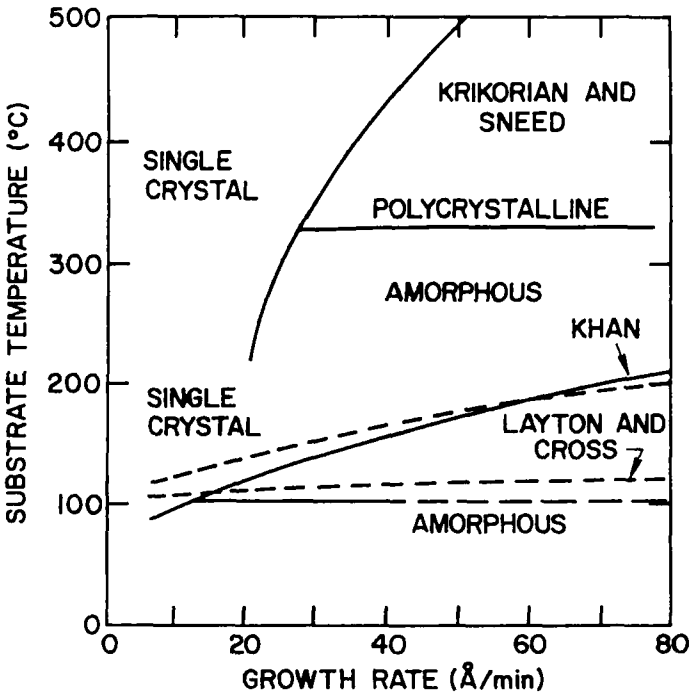

FIGURE 24. A phase map of the crystallinity of Ge films sputter deposited onto (111) Ge substrates as a function of growth rate and temperature.[229,233,235]

electron diffraction (HEED and LEED) as well as Auger electron spectroscopy (AES) were used to characterize the substrate prior to film deposition, and the effect on the epitaxial temperature of adding controlled oxygen partial pressures during film growth was investigated. AES analysis of polished and etched substrates following a vacuum system bake-out at 250°C revealed contamination by sulfur, carbon, and oxygen. However, the contaminant peaks disappeared after annealing the substrates at 625°C prior to sputter deposition, and HEED examination revealed strong Kikuchi line patterns characteristic of a clean single crystal surface. Such treatment lowered the epitaxial temperature from 300 to 145°C at a growth rate of 0.18 μm/hr.

The crystal growth results on clean substrates from Kahn's work are summarized in Figure 24 for comparison with those of Krikorian and Sneed. The transition temperatures obtained by Kahn were considerably lower and the dependence of the epitaxial temperature on the film growth rate was not as steep, leading to a lower activation energy for obtaining single crystals. This was due to an enhancement in adatom surface mobility during the nucleation and early stages of film growth caused both by the thermal regeneration of the substrate surface immediately prior to deposition and to the maintainance of a cleaner deposition environment.

Kahn demonstrated directly that the background oxygen partial pressure during deposition plays a strong role in determining the epitaxial temperature. T_e was observed to increase by 75 to 100°C in the presence of 10^{-7} to 10^{-9} Torr (10^{-5} to 10^{-7} Pa) of oxygen intentionally added through a controlled leak. In addition, T_e was 100 to 200°C higher when using Ar with 20 ppm oxygen than with Ar containing 1 ppm oxygen. AES and electron diffraction analysis indicated that oxygen was initially adsorbed on the substrate surface forming GeO_2 nuclei at activated sites such as impurity centers and dislocations.

Increased surface coverage of GeO_2 was associated with enhanced film misorientation and higher epitaxial temperatures. Under the best vacuum conditions, T_e values as low as 100°C were observed which agrees with reported results for the growth of Ge films by evaporation at similar growth rates in UHV.[234]

The effects of ion bombardment on both substrate cleaning and the reduction of impurity atom incorporation probabilities during film deposition are also illustrated in Figure 24. Layton and Cross[235] obtained results which were similar to those of Kahn while carrying out film growth in a vacuum system with a base pressure similar to that of Kirkorian and Sneed. Layton and Cross used a magnetically supported triode system operated at a target potential of −1.5 keV and an Ar pressure of 1 mTorr (0.13 Pa). Prior to deposition, the substrates, (111) oriented Ge wafers, were heated to 600°C for 10 min followed by 5 min of low energy ion bombardment. During deposition, the growing films also experienced ion bombardment due to the induced negative potential at the substrate with respect to the positive space charge region.

Haq[231] reported the effects of ion bombardment during film growth on the electrical properties of epitaxial Ge films. In his work, an asymmetric 60 Hz ac sputtering system with a base pressure of 7×10^{-6} Torr (9.3×10^{-4} Pa) was used. Sputtering was carried out in Ar at a pressure of 45 mTorr (5.9 Pa) with V_T between −2 and −3 kV and R = 1 μm/hr and resulted in an epitaxial temperature on (111) Ge substrates of 350°C. Films grown from p-type targets were always found to be p type. However, films grown from n-type targets were p type when the substrate bias V_a applied during the negative half of the cycle was low, but switched to n type at higher V_a/V_T ratios. For example, films deposited at $V_T = -3$ kV and $V_a = -0.6$ kV at 360°C were found to be n type with a room temperature carrier concentration of 3×10^{17} cm^{-3}, approximately equal to that of the target, and a near bulk electron mobility of 1930 cm^2/V-s. The effect of V_a, applied in alternate half cycles, was apparently to reduce the incorporation of acceptor species originating from contamination in the vacuum system. Capacitance-voltage measurements of such films grown on p-type substrates indicated the formation of abrupt p-n junctions.

Cadien and Greene[236] have recently reported the heteroepitaxial growth of Ge on semi-insulating (100) GaAs. The Ge/GaAs lattice mismatch is only 0.08% and very high quality Ge crystals were obtained. The films were grown in an rf diode sputtering system with a base pressure of $\sim 1 \times 10^{-7}$ Torr (1×10^{-5} Pa) using a liquid nitrogen trapped 450-ℓ/sec turbomolecular pump. Sputtering was carried out in gettered ultra-high purity Ar at P_{Ar} ranging from 5 to 25 mTorr (0.67 to 3.3 Pa) with $V_T = -760$ V. The target was an intrinsic Ge single crystal with a room temperature resistivity of >40 Ω-cm. The highly polished GaAs substrates were sputter etched at −500 V for 2 min and −250 V for 5 min at $P_{Ar} = 5$ mTorr (0.67 Pa) and T_s = 470°C immediately prior to deposition. The films were In doped p type using an evaporative In source. The incorporated In concentration was varied over two orders of magnitude by changing the applied substrate bias from 0 to −200 V. In-doped Ge films 2.7 μm thick grown at P_{Ar} = 15 mTorr (2 Pa), $V_a = 0$, R = 0.8 μm/hr, and $T_s = 513$°C exhibited room temperature hole mobilities which agree very well with those reported for bulk single crystals with comparable doping concentrations.[237] For example, μ_{hr} (300 K) = 826 cm^2/V-sec for p (300 K) = 1.2×10^{17} cm^{-3}.

2. Silicon

The majority of the work on the sputter growth of Si has been carried out using ion beam sputtering. The first reported study was by Unvala and Pearman[238] who used a 12-keV Ar^+ ion beam operated at 10^{-4} Torr (10^{-2} Pa) to obtain Si deposition rates of up to 2.4 μm/hr. Prior to deposition, the (111) Si substrates were flashed for 2 min at 1100°C in 10^{-8} Torr (10^{-6} Pa) vacuum. The authors reported a transition from polycrystalline to single crystal films at substrate temperatures between 700 and 730°C. Both n- and p-type

layers were grown and mesa diodes were fabricated with reverse breakdown voltages ranging from 30 to 150 V. Films grown on substrates held at ground potential were observed to be heavily twinned and this was attributed to stray ion bombardment. Films grown on substrates held at +9 kV were reported to exhibit no twins or stacking faults.

In a series of papers, Weissmantel and co-workers[239-242] discussed the use of ion beam sputtering for the growth of epitaxial Si films on (100) and (111) oriented spinel substrates etched with orthophosphoric acid at 350°C prior to film growth. The best results were obtained for Ar sputtering pressures of $<6 \times 10^{-6}$ Torr (8×10^{-4} Pa) and a residual gas background pressure of $<2 \times 10^{-7}$ Torr (2.7×10^{-5} Pa). A 10-keV, 15-μA Ar^+ ion beam was used to sputter a 50-mm diameter area in a 100 Ω-cm B-doped target. The film deposition rate was 0.36 μm/hr. Optimum growth temperatures for epitaxial layers on spinel were found to be between 850 and 875°C. Under these conditions 1- to 2-μm-thick films exhibited room temperature hole mobilities of ~150 cm^2/V-sec. The room temperature p-type carrier concentration of these films ranged from 1×10^{16} to 2×10^{17} cm^{-3}. Plots of carrier concentration vs. inverse temperature gave an activation energy of 50 meV which was consistent with B doping from the target. Two 8-μm-thick films were grown on (100) spinel and were found to have mobilities of ~360 cm^2/V-sec, of the same order as bulk Si with equivalent carrier concentrations. This indicated that, as expected, the films were more highly defective near the Si/spinel heterojunction resulting in lower mobilities for the thinner films. A high density of low angle grain boundaries and stacking faults was observed in all films.

Pechelyakov et al.[201] and Aleksandrov and Lovyagin[202,203] investigated the homoepitaxial nucleation of Si on vicinal (111) Si substrates using dc triode sputtering with a magnetically confined plasma. Pre-annealing the substrates at 1200 to 1300°C in gettered ultra high vacuum removed carbon contamination in the form of β-SiC particles and allowed two-dimensional layered growth at 800°C.

Rf glow discharge sputtering has been used to grow single crystal (111) Si films on (0001) sapphire from a 10^3 Ω-cm single crystal Si target.[243] The system base pressure was 10^{-6} Torr (10^4 Pa) and the deposition rate was 1.5 μm/hr. The target voltage was not specified except to be between −2 and −5 kV. The films were n type with a rather high carrier concentration of 4.8×10^{18} cm^{-3} and an electron mobility of 256 cm^2/V-sec. The authors obtained amorphous films for substrate temperatures less than 800°C, polycrystalline films between 800 and 900°C, and single crystals between 900 and 1015°C. A strong positive correlation was observed between film crystallinity and background gas purity.

3. *$Ge_{1-x}Si_x$ and Ge/Si Heterojunctions*

While some initial work has been reported on the epitaxial growth of $Ge_{1-x}Si_x$ alloys on (111) oriented Ge substrates,[244] there is considerably more interest recently, particularly by the solar energy community, in Ge/Si heterojunctions. The motivation is to grow relatively high efficiency GaAs solar cells on potentially inexpensive Ge/Si substrates. The utility of such structures depends on the ability to grow high quality epitaxial Ge films, which lattices match GaAs, on Si. However, there is an ~4% lattice mismatch between Ge and Si leading to the generation of high dislocation densities in Ge overlayers starting from abrupt heterojunctions. High dislocation and twin densities have, in fact, been observed in thin Ge films deposited on Si by electron evaporation.

The first work on sputter deposited Ge/Si heterojunctions was that of Aleksandrov et al.[245] who used a magnetically and thermionically supported dc triode system to study the nucleation of Ge on vicinal (111) Si substrates. Prior to deposition and after attaining a base pressure of 10^{-7} Torr (10^{-5} Pa), the sputtering chamber was baked at 200°C and gettered by sputtering Si from a separate target. The substrate, shielded during the Si

sputtering, was then heated to 1300°C for 10 to 20 min after which mass spectrometric analysis showed that the partial pressure of unsaturated hydrocarbons in the chamber was less than 10^{-10} Torr (10^{-8} Pa). The Ge target was cleaned by electron beam as well as by ion bombardment. The substrates were then given a final flash heating at 1300°C for 1 min prior to initiating film deposition at T_s between 480 and 590°C. The target voltage was −600 V at an Ar pressure of between 0.5 and 1 mTorr (0.007 and 0.13 Pa), allowing a deposition rate of 2.5 μm/hr. Initial film growth occurred along microsteps formed in the Si substrate during the thermal etch. At higher nominal film thicknesses, trapezoidal island formation was observed. Electrical measurements made on 2.5-μm-thick films indicated p-type conductivity with carrier concentrations between 10^{16} and 10^{17} cm^{-3} at measurement temperatures between 77 and 300 K. Room temperature hole mobilities of 600 to 1000 cm^2/V-sec were obtained.

Bajor et al.[246] have recently reported the growth of high quality 1.5-μm-thick Ge single crystals on (100) Si substrates at relatively low temperatures, 470°C, by rf diode sputter deposition. The film growth conditions were chosen to provide low energy ion bombardment of the substrate and growing film in order to produce a compositionally graded Ge/Si junction in an attempt to reduce the misfit dislocation density in the bulk film. The system base pressure was 10^{-7} Torr (10^{-5} Pa) and sputtering was carried out in gettered Ar at P_{Ar} = 15 mTorr (2 Pa) with an induced substrate potential $V_i = -65$ V. The target was an intrinsic Ge single crystal with a room temperature resistivity of $>40\ \Omega$-cm. R was 0.87 μm/hr with $V_T = -750$ V. X-ray diffraction and electron channeling spectra indicated that the films were single crystals with Hall measurements showed them to be p type with p (300 K) = 1×10^{17} cm^{-3} and corresponding carrier mobilities, 1280 cm^2/V-sec, comparable to the best bulk crystals. The net acceptor concentration was found by C-V measurements to increase from 4×10^{14} cm^{-3} at the substrate surface to the bulk film value of 1×10^{17} cm^{-3} over a ~200-nm-thick compositionally graded junction. I-V measurements on large area planar diodes indicated reverse breakdown voltages of $\geqslant 10$ V.

B. Compound Semiconductors

Sputter deposition offers certain advantages over other vapor phase techniques in controlling elemental incorporation probabilities during the growth of compound and alloy films. For example, evaporative film growth of II-VI compounds which evaporate congruently but dissociatively requires separate sources for the metal and metalloid species. Thus, three-temperature evaporation,[247] or as it is presently termed, molecular beam epitaxy,[248] is used. Furthermore, doping necessitates the use of additional sources. However, steady-state elemental sputtering rates from a compound or alloy target are independent of elemental vapor pressures, allowing the use of a single source. The provision of an overpressure of volatile species and the introduction of doping species can both be accomplished using a single two-phase source, e.g., $Ga_{0.3}Sb_{0.7}$,[139] containing the desired dopant. Alternatively, gas phase species such as AsH_3, to provide an As overpressure during the growth of GaAs, or $Al(CH_3)_3$, to provide Al as either a dopant or a host atom species, may be added to the discharge. Furthermore, low energy ion bombardment of the growing film provides additional control over elemental incorporation probabilities.

1. III-V Compounds

Detailed investigations have been carried out on the sputter deposition of InSb, GaSb, $In_{1-x}Ga_xSb$, and GaAs leading to the growth of high quality single crystals of these materials. Reported work on the growth of AlN, $Ga_{1-x}Al_xAs$, GaN, GaP, InAs, $In_{1-x}Al_xSb$, and InN is also reviewed in this section. The growth of epitaxial metastable III-V based alloys such as $InSb_{1-x}Bi_x$ and $(GaSb)_{1-x}Ge_x$ is discussed in Section V.C.

a. Antimonides

i. InSb

Most of the early work on the sputter deposition of III-V compounds was carried out on InSb[249-254] grown on cleaved NaCl. Epitaxial films were often obtained, notwithstanding the very large film/substrate lattice mismatch of ~15%, and reported values of T_e ranged from 150[254] to 320°C.[249] The films were typically n type with carrier concentrations of the order of 10^{17} cm^{-3} and electron mobilities, limited by extremely high misfit dislocation densities, of ~500 cm^2/V-sec. In one case,[250] electron mobilities as high as 13,000 cm^2/V-sec and hole mobilities of 500 cm^2/V-sec were reported for as-deposited films.

The most thorough of the early crystal growth studies was carried out by Kahn[251] who used a dc diode sputtering system with a reflection high energy electron diffraction (RHEED) attachment to investigate the growth of InSb on air-cleaved NaCl. The system base pressure was 5×10^{-7} Torr (7×10^{-5} Pa), the Ar sputtering pressure was 125 mTorr (16.7 Pa), and the target voltage was −1.25 kV. Epitaxial films, although highly twinned in [111] directions, were obtained at $T_s > 250°C$ and $R \approx 0.54$ μm/hr. Kahn reported that at these growth temperatures the intial 20 Å of deposit was tetragonal In oriented (001), [110] In ‖ (001), [110] NaCl. Additional evidence for free In formation during the early stages of InSb film growth was reported later by Greene and Wickersham.[254] At a nominal thickness of 32 nm, Kahn observed that the InSb film was a mixture of hexagonal wurtzite and cubic sphalerite phases which eventually gave way to the sphalerite polymorph at higher film thicknesses.

Greene and Wickersham[254] investigated the growth of InSb films on air-cleaved CaF_2, BaF_2, NaCl, and NaI substrates as well as on polished and annealed, (p-a), (111) oriented CaF_2. Sputter deposition was carried out at an Ar pressure of 5 mTorr (0.67 Pa) in an rf diode system with a base pressure of 5×10^{-7} Torr (7×10^{-5} Pa). The Ar sputtering gas was further purified before introducing it into the system by passing it through a Ti sponge getter heated to 900°C. The target voltage was varied between −0.3 and −1.1 kV, allowing deposition rates between 0.1 and 2.7 μm/hr. All films were approximately 0.2 μm thick. The epitaxial temperature was a function of both the substrate material and the deposition rate. For example, films grown at R = 0.12 μm/hr exhibited an epitaxial temperature of 150°C on cleaved BaF_2, which has a 4.3% lattice mismatch with InSb, as compared to T_e = 225°C on cleaved CaF_2 with a mismatch of 18.5%. In both cases the epitaxial relationship was (111), [1$\bar{1}$0] InSb ‖ (111), [1$\bar{1}$0] substrate. The epitaxial temperature increased on (p-a) CaF_2 from 175°C at R = 0.12 μm/hr to 300°C at 2.7 μm/hr. The n-type carrier concentration of films grown on (p-a) CaF_2 was of the order of 10^{17} cm^{-3}. From an analysis of the temperature dependence of the electron mobility, it was determined that the primary scattering sites were dislocations and that the charge carrier activation energy for surmounting such barriers was 40 meV.

Recently Bajor et al.[255] and Barnett et al.[256] have used the same system to grow single crystal InSb on semi-insulating (111) oriented GaAs substrates at temperatures from 300 to 475°C. The InSb/GaAs lattice mismatch is ~14%. In the latter experiments, undoped single crystal InSb wafer targets were sputtered at $V_T = -800$ V in Ar pressures ranging from 5 to 40 mTorr (0.67 to 5.3 Pa). Room temperature electron mobilities of up to 20,000 cm^2/V-sec with carrier concentrations of 3×10^{16} cm^{-3} were achieved in films grown using an applied substrate bias of $V_a = -60$ V to produce a compositionally graded junction as well as to decrease the incorporation probability of background gases. Successive chemical etching of as-deposited films followed by temperature-dependent Hall measurements showed that the electron mobility exhibited a sharp decrease near the graded InSb/GaAs interface due to the large density of misfit dislocations.

ii. GaSb

Eltoukhy and Greene[139] have grown single-crystal GaSb films on semi-insulating (100) GaAs substrates using multitarget sputtering (MTS)[168,169] to vary the Sb/Ga atomic flux ratio, r, impinging upon the growing film. The effects of systematic variations in growth variables (r, T_s, V_T, P_{Ar}, and sputtering gas purity) on the electrical properties of deposited films were evaluated. The films were p type at low temperatures with a p-to-n conversion occurring near 230°C. The room temperature hole concentration ranged from 5×10^{15} to 1×10^{18} cm^{-3} with a mobility between 1 and 100 cm^2/V-sec in 1-μm thick films.

In all cases, temperature-dependent (8- to 600-K) Hall coefficient measurements could be fitted with two acceptor levels and a net concentration of very shallow (<1 meV) acceptors. The deepest acceptor level occurred at 80 meV above the valence band edge and was associated with electrically active sites on dislocations originating at the film/substrate interface. A second acceptor level occurred at 40 meV above the valence band edge and was directly related to Sb vacancies or equivalent point defect complexes. Figures 25A and 25B show the change in concentration of this level, N_{A1}, with T_s and the Sb/Ga impingement flux ratio r. Analysis of temperature-dependent mobility data showed that the dominant charge carrier scattering sites were again dislocations introduced due to the large film/substrate lattice mismatch, ~7%.

iii. $In_{1-x}Ga_xSb$ Alloys and InSb/GaSb Superlattices

Greene et al.[167,168] first reported the growth of single crystal (In,Ga)Sb alloys as well as InSb/GaSb superlattice structures by rf multitarget sputtering.[169] In this work, two targets, one InSb and the other GaSb, were used and the substrates was continuously rotated through two electrically and physically isolated sputtering discharges. The film was thus formed by the sequential deposition of InSb and GaSb layers whose thicknesses could be adjusted from fractions of a monolayer to tens of nm. The amount of material deposited per target pass, λ, and the interlayer diffusion coefficient determined whether or not the resulting films were homogenous or compositionally modulated.

Single crystal solid solution $In_{1-x}Ga_xSb$ alloys were grown on cleaved BaF_2 at temperatures ranging from 150 to 300°C with layer thicknesses per target pass of the order of, or less than, a monolayer. Measured values of lattice constants vs. film composition obeyed Vegard's law and agreed well with bulk values. Figure 26 summarizes the structure of (In,Ga)Sb films as a function of growth temperature and film composition. Both the amorphous to polycrystalline transition and the epitaxial temperature increased with increasing mole percent GaSB. More recently, Eltoukhy and Greene[257,258] have used MTS deposition from $In_{0.3}Sb_{0.7}$ and $Ga_{0.3}Sb_{0.7}$ targets to grow single crystal $In_xGa_{1-x}Sb$ films ($0 \leqslant \times \leqslant 1$) on semi-insulating (100) GaAs substrates. From measurements carried out at 8 K, samples with $x > 0.85$ were n type, while those with $x < 0.85$ were p type. The compensation ratio was quite large for alloys with compositions near the crossover.

Single crystal InSb/GaSb superlattice structures grown by MTS have been investigated in detail by Eltoukhy and Greene.[171] The epitaxial temperature for films with layer thicknesses between 1.2 and 7 nm was found to increase with increasing modulation period Λ. The Λ dependence resulted from a decrease in the coherence between layers and the associated increased amount of plastically accommodated strain which occurred with increasing layer thickness. The critical layer thickness, h_c, for maintaining coherent interfaces in InSb/GaSb superlattice structures was determined using X-ray diffraction satellite techniques[205] and was further validated by calculating the limiting layer thickness required for bowing of threading dislocations under the misfit strain. Both methods showed that the coherent to incoherent transition for a <110> superlattice

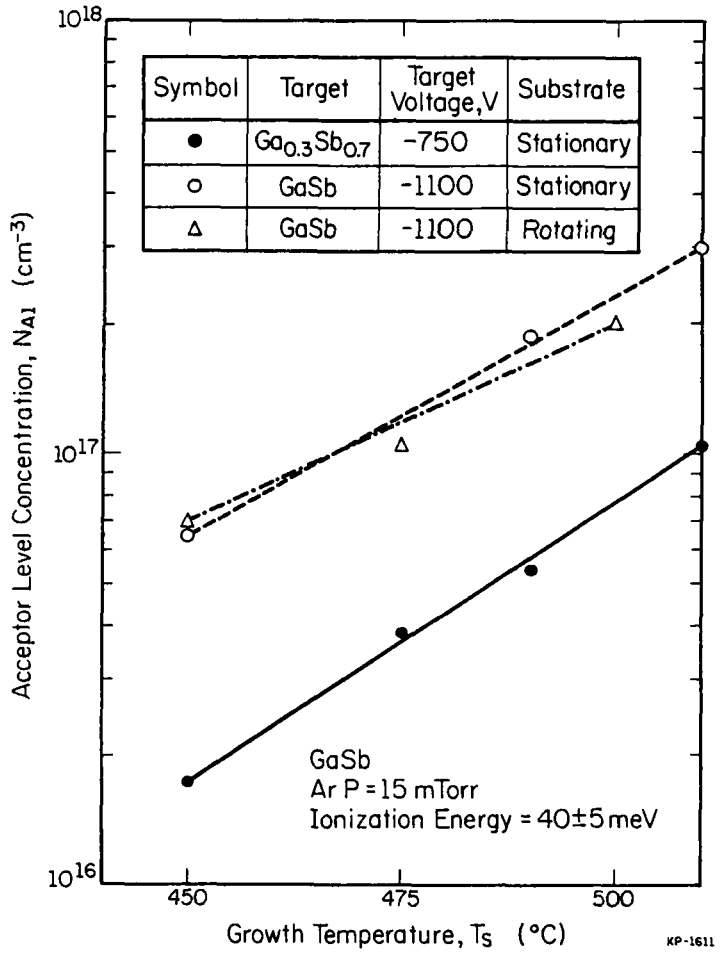

A

FIGURE 25. (A) The concentration of the acceptor level N_{A1} (located 40 meV above the valence band edge) as a function of GaSb film growth temperature using different target arrangements; (B) N_{A1} as a function of the Ga/Sb incident flux ratio during the sputter growth of GaSb films on GaAs. (From Eltoukhy, A. H. and Greene, J. E., *J. Appl. Phys.*, 50, 6396, 1979. With permission.)

modulation direction occurred at $h_c \approx 3.5$ nm. Increasing T_s and decreasing Λ also resulted in a decrease in the density of microtwins and low angle dislocation boundaries which were observed in all films.

iv. $In_{1-x}Al_xSb$

Greene et al.[167] reported the growth of epitaxial $In_{1-x}Al_xSb$ films with $0.2 < x < 0.5$ on cleaved NaCl at 400°C using multitarget rf sputtering. Alloys with substantial AlSb contents were difficult to work with since they were hygroscopic and highly reactive. The films had to be encapsulated before removing them from the vacuum system. Jachimowski and Data[259] obtained polycrystalline $In_{1-x}Al_xSb$ films by dc sputter deposition in Ar on Corning® 7059 substrates at 300°C. No electrical properties have been reported.

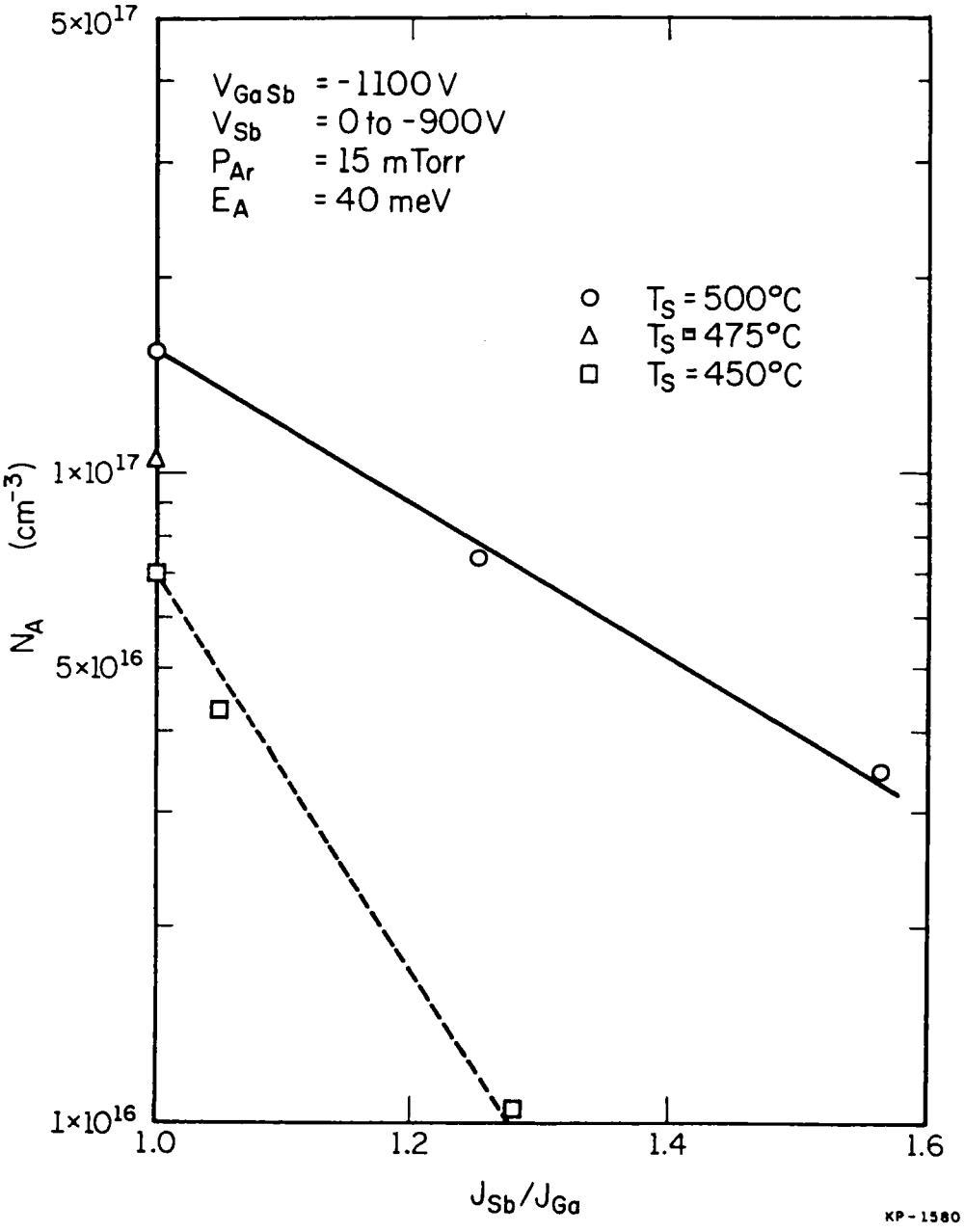

FIGURE 25B

b. Arsenides

i. InAs

Polycrystalline InAs films with rather low electron mobilities have been deposited by Ar dc sputtering in systems with poor base pressures.[260,261] Szczyrbowski et al.[261] observed some increase in μ_e due to gettering the Ar sputtering gas and applying a substrate bias during deposition. The best films had room temperature carrier concentrations of $\sim 5 \times 10^{18}$ cm^{-3} with mobilities of $\sim$500 cm^2/V-sec compared to the polycrystalline target which had $n = 5 \times 10^{16}$ cm^{-3} and $\mu_e = 1.9 \times 10^4$ cm^2/V-sec.

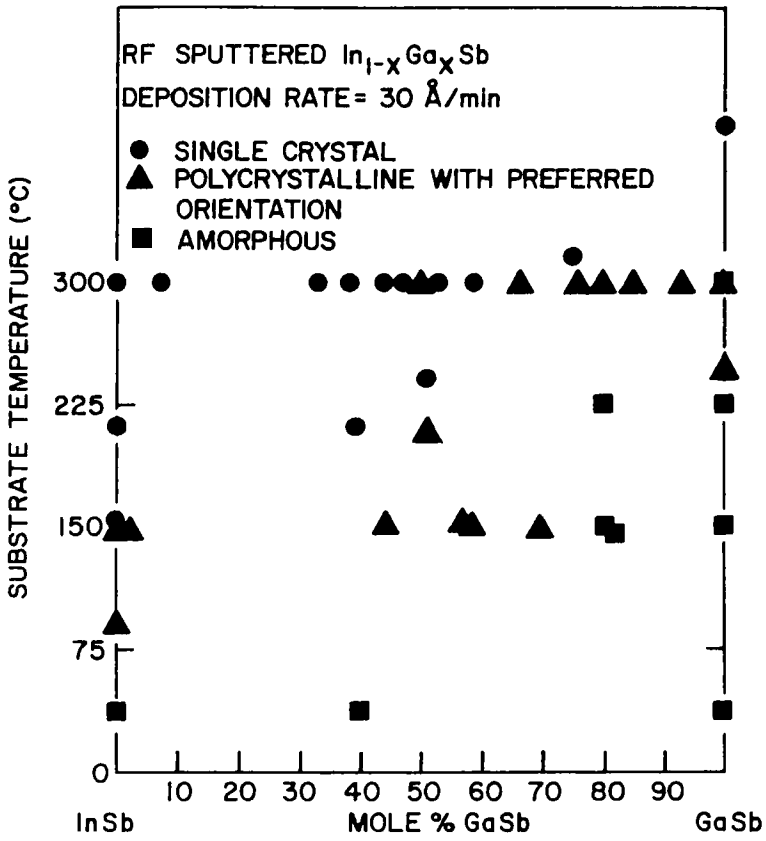

FIGURE 26. A plot showing the crystallinity of rf sputter-deposited $In_{1-x}Ga_xSb$ films on cleaved BaF_2 as a function of film composition and growth temperature. (From Greene, J. E., Wickersham, C. E., and Zilko, J. L., *J. Appl. Phys.*, 47, 2289, 1976. With permission.)

ii. GaAs and $Ga_{1-x}Al_xAs$

The early work on the sputter deposition of GaAs was carried out using either dc[262,263] or rf[264] diode sputtering in Ar from polycrystalline or pressed powder targets without supplying excess As to the growing film. The films were generally heavily twinned with epitaxy obtained only under very restricted sets of deposition conditions.

Berak and Quinn[145] used reactive rf sputter deposition to grow GaAs films in excess arsenic vapor obtained by sublimation of solid As. The target was initially liquid Ga but a skin of GaAs immediately developed under all sputtering conditions. In order to avoid condensation at surfaces other than the substrate, the entire chamber had to be maintained at a temperature at which the equilibrium vapor pressure of arsenic was greater than the sputtering pressure. The system base pressure was $\sim 2 \times 10^{-6}$ Torr (2.7×10^{-4} Pa) and the sputtering pressure was approximately 15 to 40 mTorr (2 to 5.3 Pa). Single crystal films were obtained on (0001) and ($1\bar{1}02$) oriented sapphire and (100) GaAs, but both the deposition rate and the substrate material had a large effect on the epitaxial temperature.

In their experiments, Berak and Quinn estimated that the impingement rate of As_4 vapor was 10^3 higher than that of sputtered Ga and As species. Thus, one would expect that the film growth rate in this case would be surface reaction rate limited. This was, in fact, observed; activation barriers of 0.2 to 0.35 eV were measured and the growth rate

increased with substrate temperature. Samples grown at 330°C were found by electron microprobe analysis to be arsenic rich with a composition of $Ga_{0.97\pm0.006}As_{1.027\pm0.006}$, while films grown at 490°C were stoichiometric to within experimental accuracy. Carrier mobility in all cases was less than 1 cm^2/V-sec indicating high structural defect concentrations. In a separate set of experiments, Al wire was floated on the liquid Ga target and a single crystal $Ga_{0.39}Al_{0.61}As$ film was grown on a (100) GaAs substrate at 500°C. A second single crystal film, with composition $Ga_{0.6}Al_{0.4}As$, was then grown epitaxially on the first.

The first really high quality single crystal GaAs films grown by sputter deposition were obtained recently by Barnett et al.[109] who used rf diode sputtering in excess As. Both p-type and semi-insulating films with high carrier mobilities were deposited on semi-insulating (100) GaAs substrates. The system base pressure was 10^{-7} Torr (10^{-5} Pa) while P_{Ar} ranged between 3 and 45 mTorr (0.4 and 6 Pa) with V_T between -1000 and -1500 V. The targets were undoped n-type GaAs ($n = 8 \times 10^{16}$ cm^{-3} and $\mu_e = 3100$ cm^2/V-sec) wafers and excess As was supplied to the growth interface by evaporation of crushed single crystal GaAs or 99.9999% pure As powder from an effusion oven. At the film growth temperature of 600°C, the deposition rate (~ 1 $\mu m/hr$) was controlled by the target sputtering rate. Films grown under conditions corresponding to an As/Ga impingement ratio of $\geqslant 10$ were observed to have a mirror-like featureless surface indicative of film growth in the As-stabilized mode.

Laue back reflection and dispersive double crystal[265] X-ray diffraction measurements indicated that the films were single crystals. Using the latter technique, the half-widths of the (400) diffraction peaks from the films were found to be less than those measured for the substrate, ~32 sec of arc. Undoped films were semi-insulating n type due primarily to the incorporation of oxygen which was present as a background contaminant in the discharge. Oxygen is a compensating deep donor in GaAs. The films exhibited room temperature carrier concentrations of $<10^{10}$ cm^{-3}.

Varying the applied substrate bias between 0 and -250 V resulted in changes in the incorporated oxygen concentration, as measured by secondary ion mass spectrometry, and corresponding changes in the electron mobility as shown in Figure 27. At low values of V_a, ion bombardment reduced the oxygen concentration and increased the electron mobility due to preferential sputtering from the growing film. This effect was overcome at higher values of V_a by increases in the oxygen incorporation probability due to trapping. Barnett et al.[109] also showed that the electron mobility could be further increased to 5000 cm^2/V-sec at $V_a = -100$ V by the addition of liquid nitrogen cooled shrouds to the growth chamber to reduce the background oxygen partial pressure. This represents one of the highest mobilities yet reported for semi-insulating GaAs.

Conducting p-type GaAs films were obtained by coevaporating Mn with a GaAs source in the effusion oven. Measurements of p vs. T could be fitted in the high temperature range with a single acceptor having an activation energy of 110 meV, in agreement with published values for Mn.[266] Films with, for example, room temperature hole concentrations of $p = 1.3 \times 10^{17}$ and 2.5×10^{18} cm^{-3} had corresponding mobilities of 240 and 95 cm^2/V-sec, respectively. These values agree very well with results for both LPE[267] and MBE[268] films doped to similar concentrations.

Doping of sputter-deposited GaAs films from both the gas phase and the solid phase will be discussed in more detail in Section V.D.

c. Nitrides

Some work has been carried out on the reactive sputter deposition of wide bandgap III-V nitrides from pure metal targets. System purity is extremely important because of the higher stricking probability of 0_2 than N_2 on group III elements. Small partial

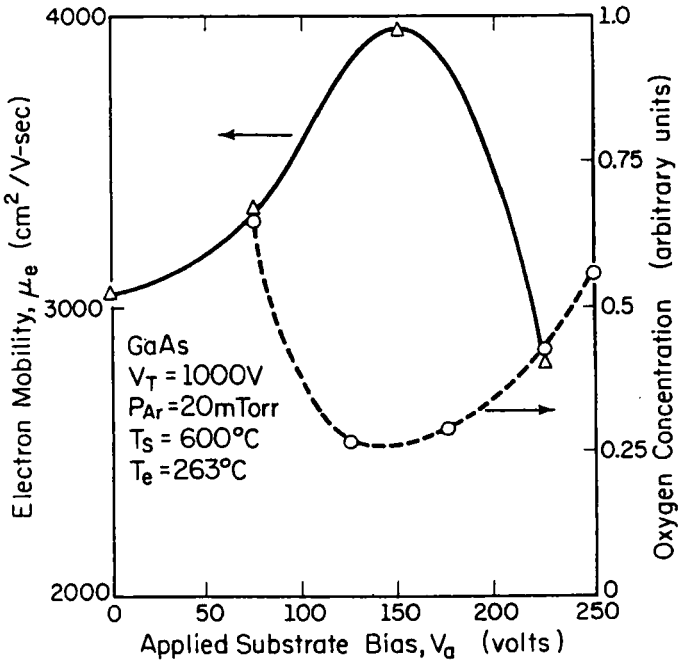

FIGURE 27. The room temperature electron mobility and the oxygen concentration in rf sputter-deposited single crystal GaAs films grown on (100) GaAs substrates as a function of substrate bias. (From Barnett, S. A., Bajor, G., and Greene, J. E., *Appl. Phys. Lett.*, 37, 734, 1980. With permission.)

pressures of oxygen result in the formation of oxynitride films as reported by Rutz et al.[269] and Natarajan et al.[149]

i. AlN

The deposition of amorphous or polycrystalline AlN layers by the reactive sputtering of Al in N_2 has been reported by several investigators.[270-272] However, either no or very little structural or chemical characterization was carried out in these studies.

Noreika et al.[273] grew polycrystalline AlN at 900°C on Ta-coated silica and single crystal Si substrates. The system base pressure was $<10^{-9}$ Torr (10^{-7} Pa) and sputtering was carried out in a static sealed module containing 80 mTorr (10.6 Pa) of Ar and 5 mTorr (0.67 Pa) of nitrogen. A controlled N_2 leak was used to replace nitrogen consumed during deposition and maintain a constant total pressure. Deposited films exhibited dielectric properties superior to bulk polycrystalline materials at temperatures up to 400°C and good high temperature stability was observed. Shuskus et al.[274] reported the growth of single crystal AlN layers on (0001) and $(01\bar{1}2)$ oriented sapphire at 1200°C by rf sputtering in ammonia. The system base pressure was 10^{-8} Torr (10^{-6} Pa), the sputtering pressure was 20 mTorr (2.7 Pa), and the film deposition rate was ~0.5 μm/hr. The observed epitaxial relationships were $(0001)_{AlN} \parallel (01\bar{1}2)_{Al_2O_3}$ with $[01\bar{1}1]_{AlN} \parallel [01\bar{1}\bar{1}]_{Al_2O_3}$. The films were piezoelectric and exhibited coupling coefficients as high as 0.2%.

ii. GaN

Semi-insulating polycrystalline GaN films have been grown by rf-reactive sputtering from Ga targets in N_2.[151,271,275]

iii. InN

Hovel and Cuomo[151] used reactive sputtering to grow polycrystalline InN films exhibiting preferred orientation on single crystal sapphire and Si substrates. The system base pressure was in the 10^{-8}-Torr (10^{-6} Pa) range before backfilling with gettered N_2 to 20 mTorr (2.7 Pa). InN films grown at T_s as high as 600°C were n type with Hall mobilities of 250 ± 50 cm^2/V-sec and carrier concentrations of 5×10^{18} to 8×10^{18} cm^{-3}.

The high temperatures at which the InN films were grown are somewhat surprising in view of the fact that InN has a very low heat of formation, 0.2 eV, and the equilibrium N_2 vapor pressure at 600°C is $\sim 15.2 \times 10^3$ Torr (2×10^6 Pa). In addition, annealing studies have shown that reactively evaporated InN films decomposed in N_2 at 500°C. The films were, however, stable in atomic N. Thus, the ability to grow InN under such seemingly unfavorable thermodynamic conditions must result from a high concentration of atomic N in the discharge. Natarajan et al.[144] and Eltoukhy et al.[150] have used optical absorption and emission spectroscopies as well as X-ray photoelectron spectroscopy to study the mechanisms of atomic N production in the discharge during reactive sputtering of In in pure N_2 and N_2 + Ar mixtures. The nitrogen concentration in the deposited films was found to depend on the position of the growth interface with respect to the negative glow region where most of the atomic N was formed through the reaction

$$N_2^* + N_2 \rightarrow N_2 + N^* + N$$

d. Phosphides

i. GaP

Polycrystalline GaP films have been deposited at elevated temperatures on glass substrates.[276,277] Sosniak[276] used both dc and rf diode sputtering to obtain p-type films with resistivities between 10 and 10^4 Ω-cm from a p-type GaP target. Starosta et al.[277] observed average grain sizes of ~0.1 μm for films grown from a sintered target by rf sputtering in Ar at T_s = 540°C. They reported no Hall response at room temperature.

2. II-VI Compounds

The majority of the published work on the use of sputter deposition to grow II-VI semiconducting films has been for direct applications as photoconducting devices (CdS, CdSe, CdTe, HgS, ZnS, and $Zn_{1-x}Cd_xS$), infrared detectors ($Hg_{1-x}Cd_xTe$), or surface acoustic wave filters (ZnO). Single crystals generally were not required, but rather polycrystalline films with preferred orientation (c-axis orthogonal to the plane of the film for wurtzite structure materials) and only moderate purity. Thus research on the crystal growth of II-VI compounds has been rather limited. Nevertheless, the growth of good quality CdS and ZnO single crystals has been reported.

a. Oxides

i. ZnO

Sputter-deposited ZnO films have been widely investigated for use in surface acoustic wave (SAW) devices. Electromechanical coupling coefficients and propagation losses closely approaching theoretical limits, for the device geometry tested, have been obtained.[278-283] Mitsuyu et al.[282] have recently reported the fabrication of a SAW filter from an epitaxial Li-doped (0001) AnO|| (0001) sapphire structure with a center frequency of 1.05 GHz.

ZnO crystallizes in the hexagonal wurtzite structure and films grown on amorphous substrates are typically polycrystalline exhibiting a small-grain columnar structure whose c axis is normal to the substrate surface. A variety of sputter deposition techniques

have been investigated for the growth of ZnO. These include dc diode reactive sputtering,[284,285] nonreactive and reactive dc sputtering from a post cathode,[286,287] dc triode reactive sputtering using a magnetically confined plasma,[288] rf diode reactive sputtering,[278,279,285,289,290] rf reactive sputtering from a hemispherical target,[280,291] and dc[292,293] and rf[282,283,294] reactive magnetron sputtering.

Of the large body of literature available on sputter-deposited ZnO, relatively little work has been reported on the detailed effects of growth parameters on microstructure and electrical properties of as-deposited films. Foster[288] observed a loss in c-axis preferred orientation when sputter depositing on evaporated metal films in the presence of substantial hydrocarbon vapor contamination. This effect was further exacerbated by the application of a substrate bias and was probably associated with discharge polymerization of the hydrocarbons. Rozgonyi and Polito[287] reported the growth of epitaxial ZnO on (0001) CdS and Al_2O_3 substrates using reactive dc sputtering from a post cathode. The system base pressure was 10^{-6} Torr (10^{-4} Pa) and the sputtering pressure was 70 mTorr (9.3 Pa). Epitaxy was obtained for $T_s \geq 300°C$ and $R \leq 0.05$ μm/hr. Film resistivity varied between 0.1 and 70 Ω-cm for Ar to O_2 partial pressure ratios >5 and between 10^4 and 10^6 Ω-cm for ratios <1. Hall mobilities were always <3 cm^2/V-sec.

Paradis and Shuskus[281] obtained single crystal ZnO films on both (0001) and $(1\bar{1}02)$ oriented sapphire substrates using magnetically confined rf sputtering from a ZnO target in a mixed 80% Ar + 20% O_2 discharge. The system base pressure was 2×10^{-6} Torr (2.67×10^{-4} Pa) and the sputtering pressure was varied from 10 to 100 mTorr (1.3 to 13.3 Pa). Figure 28 summarizes the crystal growth results as a function of R and T_s at P = 10 mTorr (1.3 Pa) for both substrate orientations. The actual number of data points was few, however the general shape of the curves was as expected (see Figure 23 and corresponding discussion). From this work, it appears that epitaxial growth proceeds more easily on $(1\bar{1}02)$ than on (0001) oriented sapphire substrates.

The results of Mitsuyu et al.[282] were similar to those of Paradis and Shuskus except that the curves were shifted to somewhat lower R and higher T_s values. Mitsuyu et al. also used rf diode sputtering but with considerably reduced longitudinal magnetic confinement and they had a lower base pressure. The films grown by Paradis and Shuskus exhibited relatively high resistivities, $>10^6$ Ω-cm, while Mitsuyu et al. could only obtain such high resistivity by sputtering from a Li-doped target and post annealing the films in air for 30 min at 600° C. As-deposited films grown by Mitsuyu from undoped targets were n type and exhibited room temperature carrier concentrations and mobilities of 1×10^{15} cm^3 and 2.6 cm^2/V-sec on (0001) oriented sapphire and 3×10^{15} cm^3 and 28 cm^2/V-sec on $(01\bar{1}2)$ sapphire.

Growth rates of up to 2 μm/hr at $210°C < T_s < 260°C$ have been reported recently for epitaxial ZnO films deposited by reactive rf planar magnetron sputtering on $(11\bar{2}0)$ sapphire substrates.[294] However, the films exhibited large optical waveguide losses.

b. Selenides

i. CdSe

Polycrystalline CdSe films have been grown on glass substrates by the reactive dc sputtering of CdSe targets in Ar + 10% H_2Se[295] and of Cd targets in selenium vapor.[296] In the latter work, Se was evaporated and mixed with a carrier gas, either H_2 or Ar, in the sputtering chamber. The photoconducting properties of the as-grown films were markedly better when Ar was used as the carrier gas. Films grown in H_2 exhibited an increase in light to dark current ratios from 10^{-2} to 10^{-7} after annealing in Ar for 1 hr at ~450° C. Lehman and Widmer[297] reported the epitaxial growth of CdSe on (0001) sapphire at 550° C by rf sputtering in Ar at 10 mTorr (1.3 Pa). The system base pressure

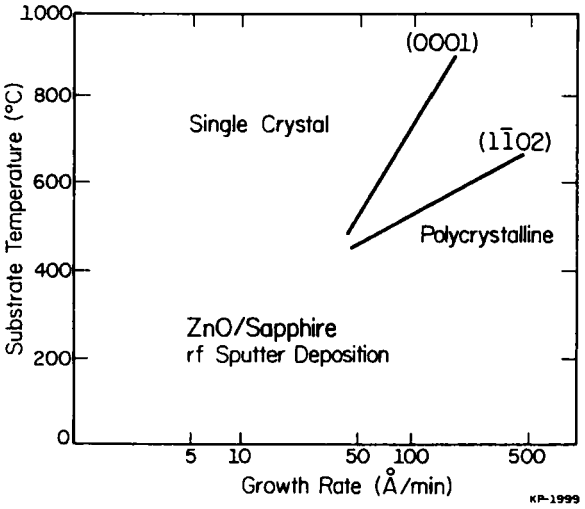

FIGURE 28. A phase map of the crystallinity of ZnO films reactively sputter deposited onto (0001) and (1$\bar{1}$02) sapphire substrates as a function of growth rate and temperature. (From Paradis, E. L. and Shuskus, A. J., *Thin Solid Films*, 38, 131, 1976. With permission.)

was 10^{-5} Torr (10^{-3} Pa). As-deposited films had a dark resistivity in excess of 10^{10} Ω-cm and a dark to light resistivity ratio of $\sim 10^3$ under a 0.1-W/cm^2 tungsten lamp illumination.

c. Sulphides

i. CdS

The earliest publications on sputtered II-VI semiconducting films report the growth of polycrystalline CdS by reactive sputtering in mixtures of Ar and H_2S[298-300] and by thermionically and magnetically supported dc sputtering in pure Ar.[250] The films were generally photoconductive and Helwig and Konig[298] reported light to dark resistance ratios of 10^4 to 10^5. Lakshamanan and Mitchell[300] measured dark resistivities of 10^6 to 10^8 Ω-cm in 0.5-μm-thick films and observed an increase in both the dark resistance and the photoresistance as the partial pressure of H_2S was increased during growth. Photoresistance decreased with In-doping of the CdS target.

Lichtensteiger et al.[301] were able to grow p-type CdS using rf diode sputtering in 10 to 30 mTorr (1.3 to 4 Pa) of Ar mixed with small partial pressures of PH_3. This was an interesting result since CdS is a nonstoichiometric n-type compound in which type conversion is difficult. Epitaxial films were obtained on (0001) oriented single crystal CdS substrates at approximately 170°C using deposition rates between 0.06 and 0.1 μm/hr. Measured carrier concentrations ranged from 1.1×10^{13} to 4.8×10^{15} cm^{-3} with corresponding Hall mobilities of 6 to 15 cm^2/V-sec. Rectifying junctions were obtained by depositing p-type CdS films on n-type CdS substrates. Film thicknesses of up to 10 μm were obtained with surface areas as large as 10 cm^2.

More recent work on the reactive sputtering of CdS in a mixed Ar + H_2S atmosphere has been reported using both CdS[146,302,303] and Cd[304] targets. Fraser and Melchoir[146] used both dc and rf diode sputtering in a system with a base pressure of 5×10^{-6} Torr (6.7×10^{-4} Pa) to deposit CdS films on glass slides covered with conducting transparent oxide electrodes. At $T_s \geq 200$°C, the growth rate was ~1 μm/hr. The film stoichiometry was

controlled by the H_2S partial pressure which was generally maintained at 2 to 6% of the total pressure, 50 mTorr (6.7 Pa). Using sputtering gas mixtures with up to 50% H_2S, it was possible to obtain films with excess S. The deposition rate decreased with increasing growth temperatures, indicating that film growth was not thermally activated. The films exhibited some basal planes preferred orientation and were photoconducting. Dark resistivities of 10^7 Ω-cm were obtained with decreases of 10^5 upon illumination with 0.5 W/cm^2 "white light". Takeuchi et al.[305] have observed photovoltaic effects in SnO_2/CdS/In sandwich structures in which the polycrystalline CdS layer was deposited by rf sputtering in pure Ar. Clarke and Greene[306] measured photoconductive gains of $\geqslant 10^4$ at 10^4 V/cm in 46-μm-thick CdS films grown on SnO_2 substrates by the reactive sputtering of Cd in a pure H_2S discharge at 20 mTorr.

ii. HgS

Nakada[307] and Nakada and Kunioka[308,309] found that thin, <200Å thick, films of HgS grown on NaCl at 250°C by rf diode sputter deposition in Ar were primarily cubic and, thus, semimetallic. Thicker films began to exhibit the desired hexagonal or semiconducting modification. Doping the pressed powder target with K, Ce, or Rb appeared to stabilize the growth of hexagonal α-HgS. Strong (0001) preferred orientation was obtained for K-doped α-HgS films grown on cleaved (111) CaF_2 in an rf Hg discharge.

iii. ZnS

Bunton and Day[264] used rf diode sputtering in Ar to deposit polycrystalline cubic β-ZnS with preferred orientation on air-cleaved NaCl. No substrate heater was used and the actual growth temperature due to plasma heating was not reported. Single crystal β-ZnS films have been obtained on (100) GaAs substrates by rf sputtering of ZnS in Ar[310] and on (100) NaCl and (100) GaAs by reactive rf sputtering of Zn in Ar + H_2S mixtures.[311] In both cases T_s ranged between ~200 and 300°C. Shonbrodt and Reichelt[311] observed mixed cubic and hexagonal phases at $T_s < 200$°C. No data were given concerning the electrical properties of the films. Durand et al.[312] reported some preliminary luminescence data for Cu and Cl-doped ZnS films grown by reactive sputtering from Zn targets in Ar + H_2S.

iv. $Zn_{1-x}Cd_xS$

Polycrystalline $Zn_{1-x}Cd_xS$ films have been deposited by reactive cosputtering from targets composed of half discs of Cd and Zn in mixed Ar + H_2S discharges.[313,314] The films were generally in the zinc blende cubic structure for small values of x, in the wurtzite hexagonal structure for large x, and of mixed phase in-between. Fraser[315] used reactive sputtering from hot pressed (Zn, Cd)S targets to deposit films with dark resistivities greater than 10^{12} Ω-cm and photoconductive gains from 0.1 to 1. The peak in the photoconductive response shifted from 488 to 400 nm with increasing ZnS concentration.

d. Tellurides

i. CdTe

Polycrystalline CdTe films which were a mixture of sphalerite cubic and wurtzite hexagonal phases[316] or cubic with a (111) preferred orientation[317] were obtained by rf diode sputtering in Ar. Pawlewkz et al.[318] was able to controllably deposit either pure cubic or pure hexagonal polycrystalline structures by growing the films in excess Te or excess Cd vapor, respectively, in an Ar rf discharge. The target was a hot pressed CdTe disc, the system base pressure was 10^{-6} Torr (10^{-4} Pa), and a typical deposition rate was 12 μm/hr (P_{Ar} and V_T were not specified). The films were highly columnar with surface feature sizes of ~1 μm on both Mo and quartz substrates at $T_s = 350$°C. Both structural

modifications exhibited high resistivities, 10^6 to 10^8 Ω-cm, with no detectable Hall voltage.

ii. $Hg_{1-x}Cd_xTe$

Zozime et al.[319,320] and Cohen-Solal et al.[321] have grown polycrystalline $Hg_{1-x}Cd_xTe$ films in the cubic modification on NaCl, mica, (111) Si, and (111) CdTe substrates using triode sputtering in a Hg discharge. Solid (CD,Hg)Te targets were used and the film composition range x = 0.2 to 0.8 was investigated. Films grown at substrate temperatures between 200 and 260° C exhibited preferred orientation. Photodiode IR detectors were prepared by cosputtering Au-doped $Cd_{0.36}Hg_{0.64}Te$ on n-type CdTe.

Recently, Cornely et al.[322] have used similar techniques to grow polycrystalline cubic $Hg_{0.75}Cd_{0.25}Te$ films with a strong (111) preferred orientation on (111) Si. The targets were cold-pressed powder discs and the system had a base pressure of 10^{-7} Torr (10^{-5} Pa). The operating conditions were $P_{Hg} \approx 1$ mTorr (0.13 Pa), $V_T = -2300$ V, $T_S = 250°$ C, and $R \approx 1.5$ μm/hr. As-deposited films were n type with a room temperature carrier concentration of $\sim 1 \times 10^{18}$ cm^{-3} and a corresponding mobility of 300 cm^2/V-sec. After annealing in an evacuated quartz ampoule at 340° C with a Hg overpressure of 560 Torr (7.4×10^4 Pa) for 14 hr, p(300 K) = 3×10^{17} cm^{-3} and μ_e (300 K) = 3000 cm^2/V-sec.

3. *IV-VI Compounds*

a. Tellurides

i. PbTe and (Pb, Sn)Te

PbTe and $Pb_{1-x}Sn_xTe$ films have been grown by Corsi[323,324] and Corsi et al.[325] using rf diode sputtering. The alloy films were deposited from two targets, (Pb, Sn)Te and Te, in order to vary the metal to Te ratio. The Ar sputtering pressure was between 0.5 and 5 mTorr (0.067 and 0.67 Pa). Observed epitaxial temperatures ranged from 250 to 350° on (111) Ge and 175 to 250° C on air-cleaved NaCl for deposition rates between 0.2 and 1 μm/hr. At 77 K, $Pb_{0.85}Sn_{0.15}Te$ films exhibited electron mobilities $>10^4$ cm^2/V-sec and carrier concentrations of approximately 10^{17} cm^{-3}. Either n- or p-type films could be obtained by controlling the metal to Te ratio. Good infrared response was observed.

Krikorian et al.[326] also investigated the sputter growth of $Pb_{1-x}Sn_xTe$. In their work they used a thermionically and magnetically supported dc sputtering system with a base pressure of 10^{-7} Torr (10^{-5} Pa). Film growth was carried out in purified Ar using cast $Pb_{1-x}Sn_xTe$ targets. They found that the film microstructure, x value (fraction of Sn on group-IV sites), carrier type, and carrier concentration were determined in a complex manner by the target x value, R, T_s, and V_s. As usual, higher structural transition temperatures were observed at larger values of R. For growth temperatures greater than about 360° C, the films were generally polycrystalline and far from stoichiometric due to decomposition. Within the epitaxial range, the film x value could be varied both above and below that of the target by systematic variations in R and T_s. Similarly, the carrier type and concentration were related to R and T_s with the p-to-n transition boundary given approximately by a hyperbola defined by a critical RT_s product.

4. *Other Semiconducting Compounds*

a. Bi_2Te_3

Francombe[327] investigated the growth of bismuth telluride by dc diode sputtering from a Bi_2Te_3 target. The system base pressure was 5×10^{-7} Torr (6.7×10^{-5} Pa) and sputtering was carried out in Ar at a pressure of 80 mTorr (10.7 Pa) with an applied target voltage of −1.5 kV. The deposition rate was ~4.8 μm/hr. Epitaxial films were obtained on (100) and (111) NaCl substrates at 400° C. However, at $T_s > 250°$ C the films were progressively more Te deficient until at 420° C the film composition was BiTe. Films grown at T_s

between 250 and 420°C exhibited metastable β-phase structures which are isostructural with Bi_2Te[3].

b. Cu_2S

The growth of orthorhombic structure chalcocite is currently of interest for application in Cu_2S/CdS heterojunction solar cells where Cu_2S is usually p type due to Cu vacancies. Cu_2S, or more typically Cu_xS ($x < 2$), layers are generally produced from CdS by a substitution reaction with CuCl in aqueous solution.[328] Recently, however, several groups have investigated the growth of Cu_2S by sputtering. The Cu-S system is complex with the formation of several compounds including CuS (covellite), $Cu_{1.8}S$ (digenite), $Cu_{1.96}S$ (djurleite), and Cu_2S. Chalcocite is also polymorphic exhibiting a phase transformation to hexagonal above $T_t = 104°C$.[329]

While there is insufficient published work as yet to sort out the detailed growth mechanisms in such a complex system, both Armantrout et al.[330] and Radler et al.[331] have demonstrated that the Cu-to-S ratio in reactively sputter-deposited films depends strongly on both T_s and V_s. Armantrout et al.[330] used rf diode sputtering of pure Cu targets in Ar + H_2S mixtures to grow orthorhombic chalcocite on glass and CdS substrates. They found that the critical partial pressure of H_2S, $P^*_{H_2S}$, decreased with the use of a positive applied substrate bias and with increasing T_s. It appears that the dominant effect of the positive substrate bias was to minimize preferential sputtering of sulfur from the growing film. The increase in the sulfur sticking probability with T_s (i.e., the decrease in $P^*_{H_2S}$) indicates a surface reaction rate limited growth mechanism.

Radler et al.[331] deposited multiphase films by rf diode sputtering from a $Cu_{1.98}S$ target sputtered in either Ar + H_2S or Ar + H_2 mixtures. Samples grown at a total pressure of 20 mTorr (2.7 Pa) with 2% H_2S always exhibited x values less than 2, but the Cu concentration increased with increasing T_s and negative substrate bias. Thus, under strongly sulfur-rich growth conditions, T_s and V_s act to decrease the sulfur incorporation probability. As expected, the Cu-to-S ratio was >2 in films deposited from $Cu_{1.98}S$ targets in reducing Ar + H_2 atmospheres. Films grown in 4% H_2 were two-phase mixtures consisting of a chalcocite matrix with Cu nodules.

A cylindrical post magnetron source was used by Jonath et al.[332] to deposit Cu_xS films from a Cu target in mixed Ar + H_2S discharges. As was the case in the work of Armantrout et al., they found that good control of P_{H_2S} was critical. Over a narrow range in P_{H_2S} at T_s values of both 35°C (less than T_t) and 130°C (above T_t), they obtained films which were primarily orthorhombic chalcocite with some djurleite. Increasing P_{H_2S} at either value of T_s lead to the formation of essentially pure djurleite. The low resistivity, primarily chalcocite, films had room temperature hold carrier concentrations ranging from 8×10^{18} cm^{-3} to 2×10^{20} cm^{-3} with a Hall mobility of ~4 cm^2/V-sec.

c. Chalcopyrites

i. $CuInS_2$

Hwang et al.[333,334] have reported the growth of polycrystalline chalcopyrite structure $CuInS_2$ films on glass slides by rf diode sputtering in Ar from pressed powder $CuInS_2$ targets. The system base pressure was 10^{-7} Torr (10^{-5} Pa) with deposition carried out at Ar pressures between 20 and 40 mTorr (2.7 and 5.3 Pa) and target biases between −2 and −3 kV. R was approximately 0.1 μm/hr. The films were p type with resistivities of the order of 0.1 to 1 Ω-cm and exhibited a strong (112) preferred orientation. The addition of excess sulfur resulted in the emergence of an additional strong diffraction peak corresponding to a (220) reflection.

ii. $CuInSe_2$

Polycrystalline $CuInSe_2$ layers with grain sizes up to 1 μm have been grown by rf sputtering from pressed powder targets.[335] The films exhibited resistivities between 0.3 and 2 Ω-cm with electron mobilities up to 6 cm^2/V-sec. CdS/$CuInSe_2$ thin film solar cells in which the CdS layers were deposited by evaporation had efficiencies of 5%.

iii. $ZnGeAs_2$

$ZnGeAs_2$ is a direct bandgap, E_g (300 K) = 1.13 eV,[336,337] chalcopyrite structure semiconductor which is of potential interest for solar cell applications. Shah and Greene[337] have recently reported the growth of the first single crystal $ZnGeAs_2$ films, by any technique, using rf diode sputtering. The system base pressure was 10^{-6} Torr (10^{-4} Pa) and sputtering was carried out in Ar at P_{Ar} = 20 mTorr (2.7 Pa). The target was a large grained polycrystalline $ZnGeAs_2$ wafer to which excess Zn had been added. Excess As was supplied to the growing film from an effusion cell similar to that used by Barnett et al.[109] for the sputter growth of GaAs. The substrates were (100) GaAs wafers and the epitaxial relationship was (0001) $ZnGeAs_2$ || (100) GaAs. The films were ~ 1 μm thick, p type, with room temperature carrier concentrations and mobilities of the order of 10^{18} cm^{-3} and 10 cm^2/V-sec, respectively.

C. Metastable Semiconductors

One of the most exciting new areas in thin film physics is the growth of single crystal metastable alloys. Such materials have unique properties and are unattainable by crystal growth techniques operating under more nearly equilibrium conditions. Other highly nonequilibrium techniques, such as splat cooling,[338] have been used to deposit metastable alloys, generally in metallic systems, but the crystalline perfection of such materials is quite poor. Ion implantation[339] and laser annealing[340] have been used to form extended solid solutions, but with the exception of work by Greene et al.[341] on the regrowth of $(GaAs)_{1-x}Ge_x$ by scanned CW laser annealing, solute solubilities are still quite limited. However, recent results using substrate-biased multitarget sputtering have demonstrated that alloys exhibiting both compositional and structural metastability can be grown as single crystals over very wide and sometimes complete concentration ranges. These materials have been found to exhibit good thermal stability.

Limitations on the growth of metastable materials are both energetic and kinetic in nature. Namely, the excess enthalpy in a metastable solid material must not exceed the enthalpy of melting, and the atomic mobility must be sufficiently low to prevent the nucleation and growth of a more stable phase. The upper limit on the allowable excess energy of a metastable phase is not a severe restriction since the enthalpy of melting is generally much larger than the energy differences between metastable and stable phases. In fact, it is because the energy differences between metastable phases are small that such materials can be grown. Low energy ion bombardment of the film during deposition provides the necessary control over elemental incorporation probabilities and adatom surface mobilities.

1. $(III\text{-}V)_{1-x}(IV)_x$ Alloys

a. $(GaAs)_{1-x}Si_x$, $(GaAs)_{1-x}Ge_x$, and $(GaSb)_{1-x}Ge_x$

$(III\text{-}V)_{1-x}(IV)_x$ alloys represent a subclass of crystalline metastable alloys which are compositionally but not structurally metastable in the sense that, unlike the InSb-InBi system discussed below in Section V.C.2, both constituents have the same space lattice. That is, III-V compounds crystallize in the zinc blende structure while Ge and Si are diamond structure.

Noreika and Francombe[342] first reported the growth of single crystal metastable semiconducting alloys using reactive sputtering in mixed Ar + SiH_4 discharges to deposit $(GaAs)_{1-x}Si_x$ from GaAs targets. The Ar pressure was maintained at 2 mTorr (0.27 Pa) while the SiH_4 partial pressure was adjusted between 0 and 1 mTorr (0.13 Pa) to obtain Si compositions ranging from 0 to 55 mol %, whereas the maximum equilibrium solubility of Si in GaAs is only ~0.5%. Epitaxy was achieved on (111) oriented GaAs substrates over the temperature range from 530 to 600°C. X-ray diffraction measurements showed that the alloys obeyed Vegard's law. Films containing more than 50% Si could be postannealed at temperatures up to 850°C before decomposing to GaAs and Si two-phase alloys.

Barnett et al.[343] have recently grown single crystal $(GaAs)_{1-x}Ge_x$ alloys on (100) GaAs by multitarget sputtering, but by far the most detailed studies yet carried out on $(III\text{-}V)_{1-x}IV_x$ were those of Cadien et al.[160,206,344] who investigated the growth and physical properties of $(GaSb)_{1-x}Ge_x$ alloys on (100) GaAs and Corning® 7059 glass substrates. The films were grown in a liquid nitrogen trapped turbomolecular-pumped MTS[169] system with a base pressure of $\sim 10^{-7}$ Torr (10^{-5} Pa). Sputtering was carried out in gettered Ar with P_{Ar} typically 15 mTorr (2 Pa). Two water-cooled targets, $Ga_{0.3}Sb_{0.7}$ and Ge, each with a purity of >99.999%, were used. The two-phase nonstoichiometric antimonide target provided excess Sb during film growth at $T_s \geq 400°C$.[139] For growth at $T_s < 400°C$, a stoichiometric GaSb target was used. V_T values ranged from −350 to −1200 V which, with a substrate rotation rate of 12 rpm, provided a deposition per target pass of from 0.1 to 0.9 monolayers.

The GaSb-Ge equilibrium phase diagram was determined by Shah et al.[345] to be a single eutectic with an invariant temperature of 648°C. The maximum solid solubilities of Ge in GaSb and GaSb in Ge occurred at this temperature and were 2 and 6.5 mol %, respectively. Nevertheless, single-phase metastable $(GaSb)_{1-x}Ge_x$ films with $0 < x < 1$ were grown at $T_s > 400°C$ and less than the transition temperature. The films were epitaxial on GaAs substrates and exhibited strong (220) preferred orientation on Corning® 7059 glass substrates. In both cases, measured lattice constants were found to obey Vegard's law.

Figure 29 shows a typical series of X-ray diffractometer (XRD) spectra taken from $(GaSb)_{0.37}Ge_{0.63}$ films grown on (100) GaAs substrates at progressively higher substrate temperatures. Only (200) and (400) alloy diffraction peaks were observed for films grown at $T_s = 470°C$, and the peak widths were limited by instrumental broadening indicating good quality single crystals. The diffraction pattern in Figure 29 shows evidence for precipitation of Ge and GaSb phases in films grown at 506°C. The matrix alloy, represented by the central peak, has become more Ge-rich with a composition of $(GaSb)_{0.31}Ge_{0.69}$. As the growth temperature was increased above 507°C, more and more precipitation was observed with the central alloy peak continuing to diminish in intensity and becoming even more Ge-rich. The side peaks, corresponding to supersaturated GaSb in Ge and Ge in GaSb phases, also moved towards the expected positions for the equilibrium phases as T_s was increased. At $T_s = 540°C$, Figure 29, the side peaks dominate but a central alloy peak is still contributing. Similar results were obtained for polycrystalline films except that at sufficiently high growth temperatures, the very strong (220) preferred orientation was lost as (111) alloy peaks appeared.

The maximum growth temperatures $T_s(max)$ at which single-phase epitaxial alloys could be obtained depended strongly, for a given alloy composition, on the degree of ion bombardment of the growing film during deposition. Even with no applied negative substrate bias V_s, the induced negative potential V_i on the growing film with respect to the positive space-charge region in the discharge was −75 V at $P_{Ar} = 15$ mTorr (2 Pa). Experiments were carried out in which the net negative bias on the growing film, $V_i + V_s$,

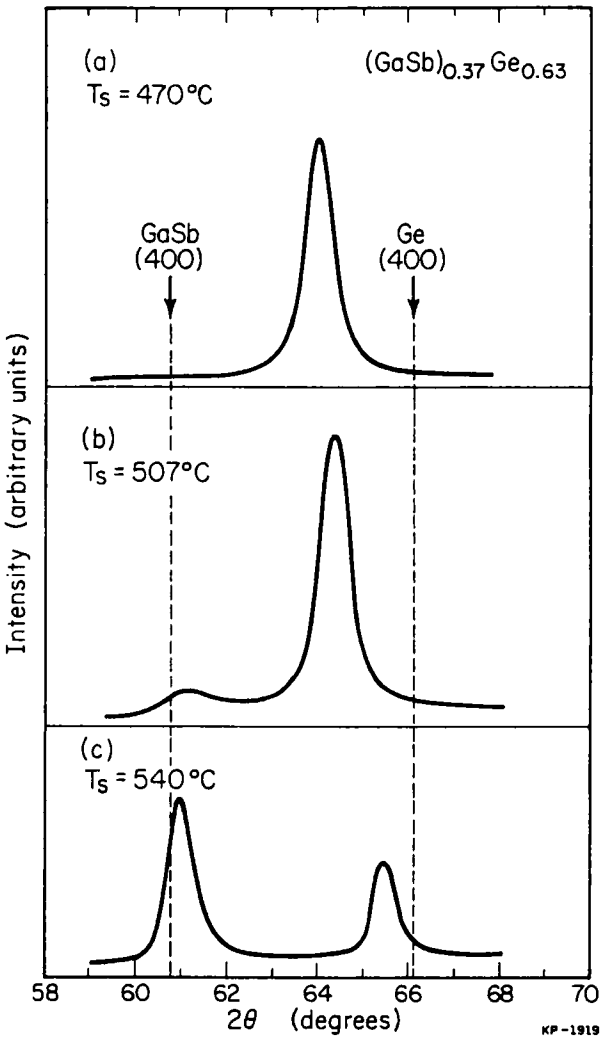

FIGURE 29. X-ray diffraction specta from $(GsSb)_{0.37}Ge_{0.63}$ alloy films grown on (100) GaAs at the temperatures indicated. The peak in (a) and the central peak in (b) are the (400) alloy reflections. The expected positions of the (400) GaSb and Ge reflections are labeled. (From Cadien, K. C., Eltoukhy, A. H., and Greene, J. E., *Appl. Phys. Lett.*, 38, 773, 1981. With permission.)

was increased by either decreasing P_{Ar} and, hence, increasing V_i or by increasing V_a directly. In both cases T_s(max) was found to increase substantially.

A summary of crystal growth results is given in Figure 30 for films grown at P_{Ar} = 15 mTorr (2 Pa) on both (100) GaAs and Corning® 7059 glass substrates. Figure 30 is a phase map plotted as a function of film growth temperature and average film composition. A three-phase region separates the single-phase metastable alloy and two-phase equilibrium fields on the phase map. The transformation from the single-phase metastable state to the equilibrium state is a continuous one. However, the narrow width of the three-phase region, ~25°C, was consistent with the large activation energies, E_a = 3.1 eV for $(GaSb)_{0.38}Ge_{0.62}$, for the phase transformation as determined from annealing results. Figure 30 also shows that the minimum in the transition temperature,

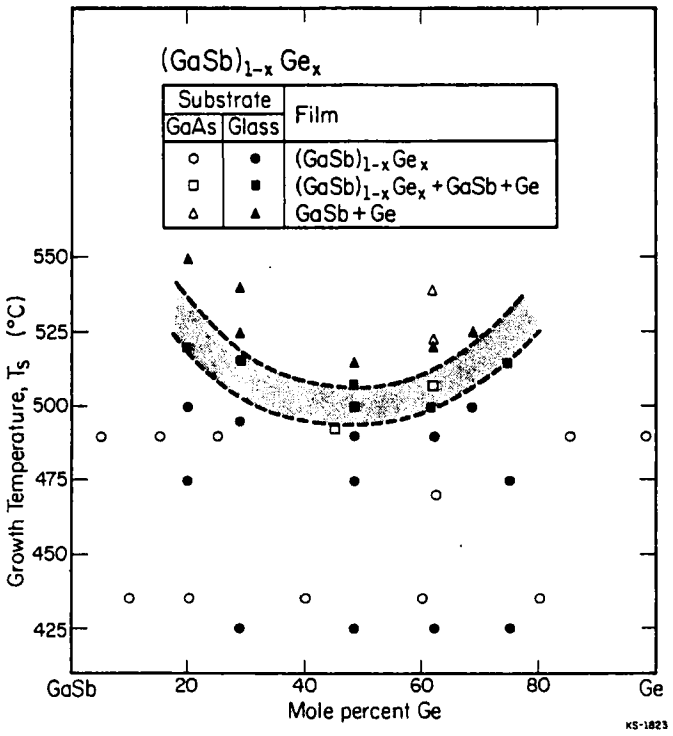

FIGURE 30. A phase map plotted as a function of growth temperature and film composition for as-deposited $(GaSb)_{1-x}Ge_x$ films grown on either (100) GaAs or Corning® 7059 glass substrates. (From Cadien, K. C., Eltoukhy, A. H., and Greene, J. E., *Appl. Phys. Lett.*, 38, 773, 1981. With permission.)

i.e., the lowest T_s(max), occurs for alloys with $x \simeq 0.5$. This is what would be predicted from the thermodynamics of regular solutions.

The transformation path for metastable $(GaSb)_{1-x}Ge_x$ alloys upon high temperature annealing proceeded through a continuous series of GaSb-rich and Ge-rich metastable phases rather than a definite intermediate state such as the one observed in $InSb_{1-x}Bi_x$.[162,346] This was indicated by the continuous shift in the angular positions of the diffracted (220) X-ray peaks during film annealing. The distinct difference in the transformation paths observed in matastable $(GaSb)_{1-x}Ge_x$ and $InSb_{1-x}Bi_x$ alloys was due to the structural constrains in the latter system.

Under the assumption that metastable $(GaSb)_{1-x}Ge_x$ alloys are regular, the interation parameter and the Gibbs free energy difference ΔG between the metastable and equilibrium states for alloys with $x = 0.5$ were calculated to be 144 and 18 meV/atom, respectively, at 300 K. The calculated value of the enthalpy for this transition in $(GaSb)_{0.36}Ge_{0.64}$ at 606°C was 33 MeV/atom which agrees very well with the experimental value obtained by differential scanning calorimetry, 27 meV/atom. Thus, the thermodynamic driving force for the metastable-to-equilibrium phase transition is relatively small while the kinetic barrier, ~3 eV, is quite large due to low self-diffusion coefficients in these alloys. This explains why the metastable phase, once formed, is stable at quite high annealing temperatures. In fact, the lifetime of these alloys at room temperature was calculated to be $\sim 10^{29}$ years.

Hall measurements carried out on single crystal $(GaSb)_{1-x}Ge_x$ fills show that all samples were p type. Room temperature carrier concentrations ranged from 10^{17} cm^{-3} for 1.5 μm thick GaSb films on GaAs to 10^{19} cm^{-3} for $(GaSb)_{0.5}Ge_{0.5}$ alloys to 10^{16} cm^{-3} for Ge on GaAs. For these same samples, room temperature hole mobilities ranged from 115 to 10 to 720 cm^2/V-sec. Lattice dynamics have been investigated recently using Raman spectroscopy.[349]

2. III-V Metastable Alloys

a. $InSb_{1-x}Bi_x$

Zilko and Greene[162,346] have carried out detailed studies on the growth mechanisms and the thermal stability of extended solubility $InSb_{1-x}Bi_x$ alloys grown on (110) GaAs substrates. $InSb_{1-x}Bi_x$ is a member of a subclass of metastable alloys which exhibit structural as well as compositional metastability. Tetragonal InBi is a semimetal whose equilibrium solid solubility in zinc blende structure InSb is 2.6 mol%. Metastable In(Sb, Bi) alloys were grown in the same MTS system described above, but with an rf-powered InSb target and a dc-powered Bi target. Low energy ion bombardment of the growing film was used to modify elemental Si and Bi incorporation probabilities, σ_{Sb} and σ_{Bi}, through preferential resputtering in order to maintain overall stoichiometry. The ion bombardment also allowed sufficient adatom mobility to grow single crystals at elevated temperatures.

The effects of the Bi to Sb impingement flux ratio J_{Bi}/J_{Sb}, T_s, and P_{Ar} on the composition and structure of the as-deposited films as well as their metastable solid solubility were investigated. Holding all growth variables except one constant in a given set of experiments, the ratio σ_{Bi}/σ_{Sb} was found to decrease with increasing J_{Bi}/J_{Sb}, increasing T_s, and decreasing P_{Ar}. However, the metastable solid solubility limit increased with decreasing P_{Ar}. Single-phase metastable films were n-type semiconductors with 100-K carrier concentrations increasing from 1.8×10^{17} to 4.5×10^{17} cm^{-3} as the mole percent of InBi was increased from 3 to 12. Electron mobilities at this temperature ranged from a few hundred to about 1000 cm^2/V-sec. The optical gap decreased with increasing InBi concentrations indicating a semiconductor-semimetal transition at ~11 mol% InBi at 20 K.

Isothermal annealing studies were carried out in order to investigate the thermal stability of $InSb_{1-x}Bi_x$ films as well as to establish a pseudobinary metastable phase diagram. The films were found to be metastable in two directions on the equilibrium In-Sb-Bi ternary phase diagram: the solid solubility of tetragonal InBi in zinc blende structure InSb was increased by more than a factor of 4 and the width of the InSb/InBi pseudobinary phase field was increased from ~0.001 to $\leqslant$0.5%. The transition from the single phase $InSb_{1-x}Bi_x$ metastable state M1 to the equilibrium state In(Sb, Bi) + InBi + Bi occurred through the intermediate metastable state M2, In(Sb, Bi) + Bi.

The metastable phase diagram was established for (110) oriented films in which it was found that the transition temperature from the M1 state to the M2 state ranged from 150 to 300°C, depending on film composition, above the equilibrium eutectic temperature and was only about 125°C less than the liquidus temperature. That is, the films exhibited no tendency to decompose during annealing runs lasting up to 125 hr for temperatures from 400 to 250°C for x ranging from 0.026 to 0.12.

D. Controlled Doping during Crystal Growth

Very little work has been reported on the controlled doping of sputter-deposited semiconductors although sputter deposition might be expected to offer advantages over other vapor phase growth techniques through the controlled use of energetic ion-surface

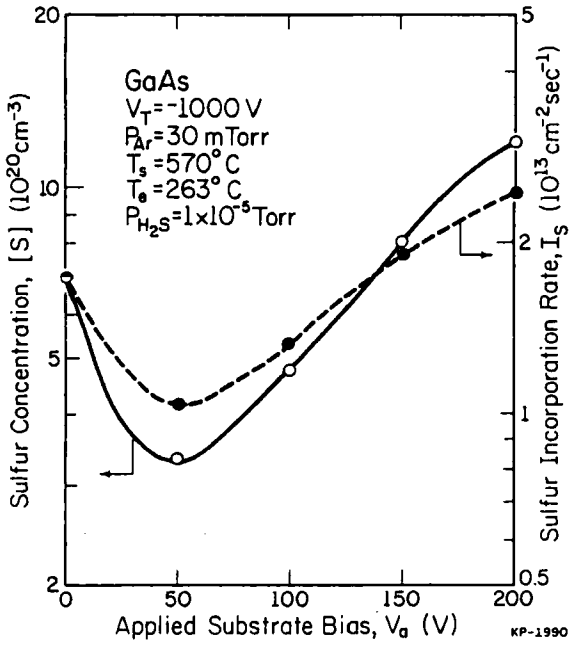

FIGURE 31. The sulfur concentration (———) and incorporation rate (— — —) in sputter-deposited single crystal GaAs films as a function of the applied substrate bias. (From Greene, J. E., Barnett, S. A., Cadien, K. C., and Ray, M. A., *J. Cryst. Growth*, 56, 389, 1982. With permission.)

interactions. In Section V.B.1.b.ii, it was pointed out that Barnett et al.[109] has used low energy ion bombardment of growing GaAs films to alter the incorporation probability of background oxygen in the films. More recently, Greene et al.[152] have carried out similar studies on the effect of ion bombardment on the incorporation probabilities of dopants added from both gas phase (H_2S) and solid phase (Sn) sources.

1. Doping from a Gas Phase Source

Sulfur doping experiments were carried out by adding partial pressures between 1×10^{-5} and 1×10^{-7} Torr (1.3×10^{-3} and 1.3×10^{-5} Pa) of H_2S to the Ar sputtering discharge during the growth of GaAs. The deposition system was the same as described previously in Section V.B.1.b.ii. An undoped single crystal GaAs wafer with $n = 8 \times 10^{16}$ cm^{-3} was used as the target and sputtering was done at a total pressure of 30 mTorr (4 Pa) with $V_T = -1000$ V. The substrates were (100) GaAs wafers maintained at 600°C. Excess As was supplied to the growing film from an As-charged effusion cell held at $T_e = 263$°C. Systematic variations in the growth parameters were made periodically during deposition. The multilayer films were then depth profiled using SIMS to determine the S concentration associated with each growth condition. The resulting S concentrations ranged from 7×10^{18} to 1.2×10^{21} cm^{-3} depending upon P_{H_2S} and V_a. For a given value of V_a, the incorporated sulfur concentration (S) was found to depend linearly on P_{H_2S} and SIMS depth profiles showed no indication of S surface segregation, although strong Te segregation has been reported in Te-doped MBE grown GaAs.[248]

The S incorporation probability was found to depend very strongly on the substrate bias. Figure 31 shows that for films grown at $V_T = -1000$ V, $P_{Ar} = 30$ mTorr (4 Pa),

$T_s = 570°C$, $T_e = 263°C$ (i.e., $As_4/Ga \simeq 5$), and $P_{H_2S} = 1 \times 10^{-5}$ Torr, the sulfur concentration [S] initially decreased with increasing substrate bias, reached a minimum near $V_a = -50$ V, and increased with further increases in V_a. These results agree qualitatively with those shown in Figure 27 for 0-doping. The minimum in both cases is due to the addition of two competing effects: preferential sputtering of dopant from the growing film surface, primarily by reflected Ar neutrals and accelerated Ar^+ ions, and trapping of accelerated dopant-containing species. The trapping probability is temperature dependent and requires chemical bonding of the very shallowly implanted species with the matrix. This explains why no Ar was detected in the films by either SIMS or electron microprobe analysis, even though the Ar concentration in the discharge was several orders of magnitude larger than the total sulfur concentration.

The dominance of sputtering over trapping at low values of V_a was due to the sputtering threshold being on the order of 25 eV, while the trapping threshold is ~100 eV for S in GaAs. Under these growth conditions, the thermal sticking probability of S was $\phi_S = 0.008$ while the incorporation probability due to trapping was essentially unity for $V_a \geqslant 200$ V.

2. Doping from a Solid Phase Source

Sn doping[152] was achieved by cosputtering from a GaAs + Sn target where the steady-state Sn/Ga impingement flux ratio was 0.001. This corresponds to a doping concentration of $[Sn] = 2 \times 10^{19}$ cm^{-3} if $\sigma_{Sn} = 1$. As in the S doping experiments, a series of layers were grown at different values of V_a in one vacuum pumpdown and the multilayer films analyzed by SIMS. Although ϕ_{Sn} was essentially unity for the growth temperature used, $T_s = 570°C$, Figure 32 shows that for $V_a = 0$, the measured Sn concentration in as-doposited films was only 1.2×10^{19} cm^{-3}. Some Sn was lost due to sputtering from the growing film due to the induced potential V_i on the substrate with respect to the positive space charge region in the plasma. In these experiments, V_i was ~65 V. Increasing V_a, algebraically additive to V_i, resulted in a monotonically decreasing Sn concentration. The magnitude of this decrease was considerably larger than for the case of S-doping.

The large loss in Sn incorporation by sputtering was due to an enhanced surface Sn coverage θ_{Sn} caused by surface segregation during film growth. SIMS measurements showed that θ_{Sn} was always much larger than the bulk concentration [Sn], an effect also observed for Sn doping in MBE-grown GaAs.[347,348] However, θ_{Sn} was more than two orders of magnitude less in sputter-grown than in MBE-grown films due to collisional mixing and recoil implantation induced by the low energy ion bombardment (see discussion in Reference 350).

VI. CONCLUSIONS

The key feature which distinguishes sputtering from other vapor phase growth techniques is the bombardment of the substrate and growing film with energetic particles (host lattice species, dopants, and/or inert gas ions) during deposition. It was demonstrated in Sections IV and V that such energetic particle-surface interactions affect every phase of film deposition and allow additional control over nucleation and growth kinetics, elemental incorporation probabilities, and film chemistry.

It is clear from the literature review in Section V that sputter deposition offers tremendous versatility in the growth and controlled doping of high quality single crystals. Equally clear, however, is that a great deal more fundamental research in understanding film growth and dopant incorporation kinetics is still required before sputter deposition can achieve its potential. In addition, more attention needs to be given to the technology

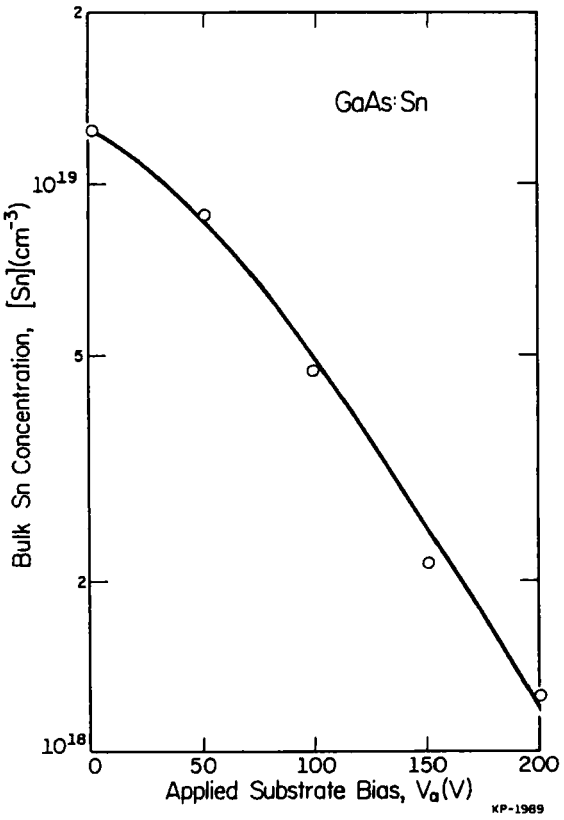

FIGURE 32. The Sn concentration in sputter-deposited single crystal GaAs films as a function of the applied substrate bias. (From Greene, J. E., Barnett, S. A., Cadien, K. C., and Ray, M. A., *J. Cryst. Growth*, 56, 389, 1982. With permission.)

of sputter growth, for example, in the design and use of ultra-high vacuum ion beam systems and in developing cleaner gas handling capabilities.

ACKNOWLEDGMENTS

The author gratefully acknowledges the financial support of the Joint Services Electronics Program under contract N00014-79-C-0424 and the Department of Energy contract DE-AC02-76ER01198 during the course of this work. In addition, I am particularly grateful for the encouragement, suggestions, and friendly criticisms of the University of Illinois research effort in crystal growth over a number of years by Drs. John Dimmock and George Wright of the Office of Naval Research.

REFERENCES

1. **Grove, W. R.**, On the electro-chemical polarity of gases, *Trans. Royal Soc.*, 142, 87, 1852.
2. **Itoh, N.**, Sputtering and dynamic interstitial motion in alkali halides, *Nuclear Instrum. Methods*, 132, 201, 1976.
3. **Townsend, P. D.**, Photon induced Sputtering, *Surf. Sci.*, 90, 256, 1979.
4. **Townsend, P. D., Browning, R., Garlant, D. J., Kelley, J. C., Mahjoobi, A., Michael, A. J., and Saidoh, M.**, Sputtering patterns and defect formation in alkali halides, *Rad. Eff.*, 30, 55, 1976.

5. **Overeijnder, H. Szymonski, M., Haring, A., and deVries, A. E.,** Electron sputtering of alkali halides. A study of its dependence on the beam energy and the target temperature, *Rad. Eff.*, 38, 21, 1978.
6. **Szymonski, M.,** On the model of the electron sputtering process of alkali halides, *Rad. Eff.*, 52, 9, 1980.
7. **McCracken, G. M.,** The behavior of surfaces under ion bombardment, *Rep. Prog. Phys.*, 28, 241, 1975.
8. **Hagstrum, H. D.,** Low energy de-excitation and neutralization processes near surfaces, in *Inelastic Ion-Surface Collisions,* Talk, N. H., Tully, J. C., Heiland, W., and White, C. W., Eds., Academic Press, New York, 1977, chap. 1.
9. **Petrov, N. N.,** Secondary emission from incandescent metal bombarded by cesium and potassium ions, *Sov. Phys. Sol. St.*, 2, 865, 1960.
10. **Wehner, G.,** Energievertelilung der von 2, 5, 10 und 15 keV He- und Ar-Ionen an Molybdän ausgelöten Eletronen, *Z. Phys.*, 193, 439, 1966.
11. **Kornelsen, E. V.,** The ionic entrapment and thermal desorption of inert gases in tungsten for kinetic energies of 40 eV to 5 keV, *Can. J. Phys.*, 42, 364, 1964.
12. **Carter, G., Armour, D. G., Donnelly, S. E., Ingram, D. C., and Webb, R. P.,** The injection of inert gas ions into solids: their trapping and escape, *Rad. Eff.*, 53, 143, 1980.
13. **Oechsner, H.,** Sputtering — A review of some recent experimental and theoretical aspects, *Appl. Phys.*, 8, 185, 1975.
14. **Kornelsen, E. V. and Sinha, M. K.,** Thermal release of inert gases from (110) and (211) tungsten surfaces, *J. Appl. Phys.*, 40, 2888, 1969.
15. **Harrison, D. E., Kelly, P. W., Garrison, P. J., and Winograd, N.,** Low energy ion impact phenomena on single crystal surfaces, *Surf. Sci.*, 76, 311, 1978.
16. **Wehner, G. K. and Anderson, G. S.,** The nature of physical sputtering, in *Handbook of Thin Film Technology,* Maissel, L. I. and Glang, R., Eds., McGraw-Hill, New York, 1970, chap. 3.
17. **Stuart, R. V. and Wehner, G. K.,** Sputtering yields at very low bombarding ion energies, *J. Appl. Phys.*, 33, 2345, 1962.
18. **Sigmund, P.,** Theory of sputtering. I. Sputtering yield of amorphous and polycrystalline targets, *Phys. Rev.*, 184, 383, 1969.
19. **Wehner, G. K., Stuart, R. V., and Rosenburg, D.,** General Mills Annual Report of Sputtering Yields, Number 2254, 1961.
20. **Guseva, M. I.,** The sputtering effect of positive ions with energies up to 25 keV in a small electromagnetic separator, *Sov. Phys. Sol. St.*, 1, 1410, 1960.
21. **Almen, O. and Bruce, G.,** Collection and sputtering experiments with noble gas ions, *Nucl. Instrum. Methods,* 11, 257, 1961.
22. **Dupp, G. and Scharmann, A.,** Die Zerstäubung von Kupfer durch Ne^+–, Ar^+–, Kr^+– und Xe^+– Ionen im Energiebereich von 75 keV bis 1 MeV, *Z. Physik,* 192, 284, 1966.
23. **Keywell, F.,** Measurements and collision — radiation damage theory of high-vacuum sputtering, *Phys. Rev.*, 97, 1611, 1955.
24. See, for example, **Hous, M. and Robinson, M. T.,** Computer simulation of low energy sputtering in the binary collision approximation, *Appl. Phys.*, 18, 381, 1979, and references therein.
25. See for example, **Winograd, N., Garrison, J., Fleisch, T., Delgass, W. N., and Harrison, D. E.,** Particle ejection from ion-bombarded clean and reacted single crystal surfaces, *J. Vac. Sci. Technol.*, 16, 629, 1979.
26. **Sigmund, P.,** Collision theory of displacement damage, ion ranges, and sputtering, *Rev. Roum. Phys.*, 17, 832, 1972.
27. **Sigmund, P.,** Collision theory of displacement damage: displacement cascades, *Rev. Roum. Phys.*, 17, 969, 1972.
28. **Sigmund, P.,** Collision theory of displacement damage: some aspects of sputtering, *Rev. Roum. Phys.*, 17, 1079, 1972.
29. **Winterbon, K. B.,** *Ion Implantation Range and Energy Deposition Distributions,* Vol. 2, Plenum Press, New York, 1975.
30. **Bay, H. L. and Bohdansky, J.,** Sputtering yields for light ions as a function of angle of incidence, *Appl. Phys.*, 19, 421, 1979.
31. **Sigmund, P.,** in *Proceedings of the Int. Conf. on Atomic Collisions in Solids,* Kiev, 1974.
32. **Gurmin, B. M., Ryzhov, Yu. A., and Skharban, I. I.,** Angular distributions of atoms sputtering from polycrystalline targets by inert-gas ions, *Bull. Acad. Sci. USSR, Phys. Ser. (USA),* 33, 752, 1969.
33. **Wehner, G. K. and Rosenberg, D.,** Angular distribution of sputtered material, *J. Appl. Phys.*, 31, 177, 1960.
34. **Patterson, H. and Tomlin, D. H.,** Experiments by radioactive tracer methods on sputtering by rare-gas ions, *Proc. Roy. Soc.*, 265, 474, 1962.
35. **Littmark, U. and Sigmund, P.,** Momentum deposition by heavy-ion bombardment and an application to sputtering, *J. Phys. D.*, 8, 241, 1975.

36. **Matsunami, N., Yamamura, Y., Itakawa, Y., Itoh, N., Kazumata, Y., Miyagawa, S., Morita, K., and Shimizu, R.,** A semi-empirical formula for the energy dependence of the sputtering yield, *Rad. Eff. Letters*, 57, 15, 1980.
37. **Bohdansky, J., Roth, J., and Bay, H. L.,** An analytical formula and important parameters for low energy ion sputtering, *J. Appl. Phys.*, 52, 2861, 1980.
38. **Stuart, R. V. and Wehner, G. K.,** Sputtering thresholds and displacement energies, *Phys. Rev. Lett.*, 4, 409, 1960.
39. **Husinsky, W. Bruckmüller, R., Blum, P., Viehböck, F., Hammer, D., and Benes, E.,** Measurements of the velocity spectrum of sputtered Na from a NaI target by a Doppler-shift laser spectrometer, *J. Appl. Phys.*, 48, 4734, 1977.
40. **Overeijnder, H., Haring, A., and deVries, A. E.,** The sputtering processes of alkali halides during 6 keV Xe^+ ion bombardment, *Rad. Eff.*, 37, 205, 1978.
41. **Husinsky, W. and Bruckmüller, R.,** Energy spectra of sputtered Na atoms from bombardment of NaCl with 20 keV rare gas ions, *Surf. Sci.*, 80, 637, 1979.
42. **Johson, R. E. and Evatt, R.,** Thermal spikes and sputtering yields, *Rad. Eff.*, 52, 187, 1980.
43. **Thompson, D. A.,** Non-linear effects in sputtering, in *Proceedings of the Symposium on Sputtering*, Varga, P., Betz, G., and Viehböck, F. P., Eds., Inst. Allgemeine Physik, Technische Universität Wein, Austria, 1980, 62.
44. **Sigmund, P.,** Sputtering of single and multiple component materials, *J. Vac. Sci. Technol.*, 17, 396, 1980.
45. **Bay, H. L., Andersen, H. H., Hofer, W. O., and Nielsen, O.,** The energy dependence of gold selfsputtering, *Nucl. Instrum. Methods*, 132, 301, 1976.
46. **Andersen, H. H. and Bay, H. L.,** Heavy-ion sputtering yields of gold: further evidence of non-linear effects, *J. Appl. Phys.*, 46, 2416, 1975.
47. **Andersen, H. H. and Bay, H. L.,** Nonlinear effects in heavy-ion sputtering, *J. Appl. Phys.*, 45, 953, 1974.
48. **Johar, S. S. and Thompson, D. A.,** Spike effects in heavy-ion sputtering of Ag, Au, and Pt thin films, *Surf. Sci.*, 90, 319, 1979.
49. **Oliva-Florio, A. R., Alonson, E. V., Baragiola, R. A., Ferron, J., and Jakas, M. M.,** Energy dependence of the molecular effect in sputtering, *Rad. Eff. Letters*, 50, 3, 1979.
50. **Veje, E.,** Emission of secondary electrons and photons from silver bombarded with Sb^+, Sb_2^+, and Sb_3^+, *Rad. Eff. Letters*, 58, 35, 1981.
51. **Thum, F. and Hofer, W. O.,** No enhanced electron emission from high-density atomic collision cascades in metals, *Surf. Sci.*, 90, 331, 1979.
52. **Anderson, C. A. and Hinthorne, J. R.,** Ion microprobe mass analyzer, *Science*, 175, 853, 1972.
53. **Benninghoven, A. and Mueller, A.,** Secondary ion yields near 1 for some chemical compounds, *Phys. Letters*, 40A, 169, 1972.
54. **Werner, H. W.,** The use of secondary ion mass spectrometry in surface analysis, *Surf. Sci.*, 47, 301, 1975.
55. **Benninghoven, A.,** Developments in secondary ion mass spectroscopy and applications to surface studies, *Surf. Sci.*, 53, 596, 1975.
56. **Williams, P.,** Materials Research Laboratory, University of Illinois, private communication.
57. **Oechsner, H. and Gerhard, W.,** Mass spectroscopy of sputtered neutrals and its application for surface analysis, *Surf. Sci.*, 44, 480, 1974.
58. **Gerhard, W. and Oechsner, H.,** Mass spectrometry of neutral molecules sputtered from polycrystalline metals by Ar^+-ions of 100—1000 eV, *Z. Physik*, B22, 41, 1975.
59. **Gerhard, W.,** A model calculation of the neutral molecule emission by sputtering processes, *Z. Physik*, B22, 31, 1975.
60. **Winograd, N., Harrison, D. E., Jr., Garrison, B. J.,** Structure sensitive factors in molecular cluster formation by ion bombardment of single crystal surfaces, *Surf. Sci.*, 78, 467, 1978.
61. **Können, G. P., Tip, A., and deVries, A. E.,** On the energy distribution of sputtered dimers, *Radiat. Eff.*, 21, 269, 1974.
62. **Konnen, G. P., Tip, A., and deVries, A. E.,** On the energy distribution of sputtered clusters, *Radiat. Eff.*, 26, 23, 1975.
63. **Garrison, B. J., Winograd, N., and Harrison, D. E., Jr.,** Formation of small metal clusters by ion bombardment of single crystal surfaces, *J. Chem. Phys.*, 69, 1440, 1978.
64. **Prigge, S. and Bauer, E.,** Static SIMS studies of metal covered W(110) surfaces, in *Proc. 2nd Int. Conf. Secondary Ion Mass Spectrometry*, Benninghoven, A., Evans, C. A. Jr., Powel, R. A., Shimizu, R., and Storms, H. A., Eds., Springer-Verlag, New York, 1979, 133.
65. **Coburn, J. W., Taglauer, E., and Kay, E.,** a study of the neutral species of sputtered from oxide targets, I, *Japn. J. Appl. Phys.* Suppl. 2, 501, 1974.

66. **Gruen, D. M., Guadioso, S. L., McBeth, R. L., and Kerner, J. L.,** Application of matrix isolation spectroscopy to quantitative sputtering studies. I. Energies and oscillator strengths of the resonance transitions of gold atoms isolated in noble gas matrices, *J. Chem. Phys.*, 60, 89, 1974.
67. **Gruen, D. M., Finn, P. A., and Page, D. L.,** Vaporization thermodynamics and molecular sputtering of binary targets, *Nucl. Technol.*, 29, 309, 1976.
68. **Steinbruchel, Ch. and Gruen, D. M.,** Absolute measurement of sputtered ion fractions using matrix isolation spectroscopy, *Surf. Sci.*, 93, 299, 1980.
69. **Comas, J. and Cooper, C. B.,** Mass spectrometric study of sputtering of single crystals of GaAs by low energy Ar ions, *J. Appl. Phys.*, 38, 2956, 1967.
70. **Szymonski, M. and Bhattacharya,** The sputtering of GaAs at elevated temperatures, *Appl. Phys.*, 20, 207, 1979.
71. **Stuart, R. V., Wehner, G. K., and Andersen, G. S.,** Energy distribution of atoms sputtered from polycrystalline metals, *J. Appl. Phys.*, 40, 803, 1969.
72. **Oechsner, H.,** Enerieverteilung bei der Festkorperzerstäubung durch Ionenbeschuβ, *Z. Physik*, 238, 433, 1970.
73. **Bernhardt, F., Oechsner, H., and Stumpe, E.,** Energy distributions of neutral atoms and molecules sputtered from polycrystalline silver, *Nuc. Inst. Methods*, 132, 329, 1976.
74. **Gillam, E.,** The penetration of positive ions of low energy into alloys and composition changes produced in them by sputtering, *J. Phys. Chem. Solids*, 11, 55, 1959.
75. **Andersen, H. H.,** Sputtering of multicomponent metals and semiconductors, in *Symposium on the Physics of Ionized Gases 1980*, Cobic, B., Ed., Boris Kidric Institute of Nuclear Sciences, Beograd, Yugoslavia, 1981.
76. **Coburn, J. W.,** The influence of ion sputtering on the elemental analysis of solid surfaces, *Thin Solid Films*, 64, 371, 1979.
77. **Patterson, W. L. and Shirn, G. A.,** The sputtering of nickel-chromium alloys, *J. Vac. Sci. Technol.*, 4, 343, 1967.
78. **Shimizu, H., Ono, M., and Nakayama, K.,** Quantitative Auger analysis of copper-nickel alloy surfaces after argon ion bombardment, *Surf. Sci.*, 36, 817, 1973.
79. **Ho, P. S., Lewis, J. E., Wildman, H. S., and Howard, J. K.,** Auger study of preferred sputtering on binary alloy surfaces, *Surf. Sci.*, 56, 393, 1976.
80. **Winters, H. F. and Coburn, J. W.,** Influence of the altered layer on depth profiling measurements, *Appl. Phys. Letters*, 28, 176, 1976.
81. **Pickering, H. W.,** Ion sputtering of alloys, *J. Vac. Sci. Technol.*, 13, 618, 1976.
82. **Ho, P. S.,** Effects of enhanced diffusion of preferred sputtering of homogeneous alloy surfaces, *Surf. Sci.*, 72, 253, 1978.
83. **Webb, R., Carter, G., and Collins, R.,** The influence of preferential enhanced diffusion on composition changes in sputtered binary solids, *Rad. Effects*, 39, 129, 1978.
84. **Lam, N. Q., Leaf, G. K., and Wiedersich, H.,** Sputter-induced surface composition changes in alloys, *J. Nuc. Mat.*, 88, 289, 1980.
85. **Eltoukhy, A. H. and Greene, J. E.,** Diffusion enhancement due to low-energy ion bombardment during sputter etching and deposition, *J. Appl. Phys.*, 51, 4444, 1980.
86. **Greene, J. E., Natarjan, B. R., and Sequeda-Osorio, F.,** Sputtering of metal alloys containing second phase precipitates, *J. Appl. Phys.*, 49, 417, 1978.
87. **Andersen, N. and Sigmund, P.,** Energy dissipation by heavy ions in compound targets, *K. Dan. Vidensk. Selsk. Mat. Fys. Medd.*, 39, Number 3, 1, 1974. (See also reference 75.)
88. **Liau, Z. L., Brown, W. L., Homer, R., and Poate, J. M.,** Surface-layer composition changes in sputtered alloys and compounds, *Appl. Phys. Letters*, 30, 626, 1977.
89. **Tarng, M. L. and Wehner, G. K.,** Alloy sputtering studies with in-situ Auger electron spectroscopy, *J. Appl. Phys.*, 42, 2449, 1971.
90. **Taglauer, E. and Heiland, W.,** Changes in the surface composition of compounds due to light ion bombardment, in *Symposium on Sputtering*, Varga, P., Betz, G., Viehböck, F. P., Eds., Inst. Allegemein, Physik, Vienna, 1980, 423.
91. **Sigmund, P.,** Sputtering processes: collision cascades and spikes, in *Inelastic Ion-Surface Collisions*, Tolk, N. H., Tully, J. C., Heiland, W., and White, C. W., Eds., Academic Press, New York, 1977, p. 121.
92. **Sigmund, P.,** Sputtering by ion bombardment, in *Topics in Applied Physics*, Vol. 47, Behrisch, R., Ed., Springer, in press.
93. **Russell, W. A. Papanastassiou, D. A., and Tombrello, T. A.,** Kellogg Rad. Lab. Report BAP-19, 1980. (See also reference 75.)
94. **van Oostrom, A.,** Application of AES to the study of selective sputtering of thin films, *J. Vac. Sci. Technol.*, 13, 224, 1976.

95. **Jacobi, K. and Ranke, W.,** Oxidation and annealing of GaP and GaAs (111) faces studied by AES and UPS, *J. Electron. Spectros. Rel. Phen.*, 8, 225, 1976.
96. **Singer, I. L., Murday, J. S., and Comas, J.,** Preferential sputtering from disordered GaAs, *J. Vac. Sci. Technol.*, 18, 161, 1981.
97. **Mizokawa, Y., Iwasaka, H., Nishitani, R., and Nakamura, S.,** ESCA studies of Ga, As, GaAs, Ga_2O_3, and As_2O_5, *J. Electron. Spectros. Rel. Phen.*, 14, 129, 1978.
98. **McGuire, G. E.,** Effects of ion sputtering on semiconductor surfaces, *Surf. Sci.*, 76, 130, 1978.
99. **Singer, J. L., Murday, J. S., and Cooper, L. R.,** Abstract: Composition changes in GaAs due to low energy ion bombardment, *J. Vac. Sci. Technol.*, 15, 127, 1978.
100. **Eltoukhy, A. H., Barnett, S. A., and Greene, J. E.,** Ion bombardment effects on elemental incorporation probabilities during sputter deposition of GaSb and InSb, *J. Vac. Sci. Technol.*, 16, 321, 1979.
101. **Zilko, J. L., Barnett, S. A., Eltoukhy, A. H., and Greene, J. E.,** Modification of elemental incorporation probabilities by ion bombardment during growth of III-V compound and metastable films, *J. Vac. Sci. Technol.*, 17, 595, 1980.
102. **Stewart, A. D. G. and Thompson, M. W.,** Microtopography of surfaces eroded by ion-bombardment, *J. Materials Sci.*, 4, 56, 1969.
103. **Barber, D. J., Frank, F. C., Moss, M., Steeds, J. W., Tsong, I. S. T.,** Prediction of ion-bombardment surface topographies using Frank's kinematic theory of crystal dissolution, *J. Materials Sci.*, 8, 1030, 1973.
104. **Frank, F. C.,** On the kinematic theory of crystal growth and dissolution processes, in *Growth and Perfection of Crystals*, Doremus, R. H., Roberts, B. W., and Turnbull, D., Eds., Wiley, 1958, 411.
105. **Carter, G., Colligon, J. S., and Nobes, M. J.,** Analytical modelling of sputter induced surface morphology, *Rad. Eff.*, 21, 65, 1977.
106. **Belson, J. and Wilson, I. H.,** Flux density equations for topographical evolution of features on ion bombarded surfaces, *Rad. Eff.*, 51, 27, 1980.
107. **Wilson, I. H.,** The topography of sputtered semiconductors, *Rad. Eff.*, 18, 95, 1973.
108. See, for example, **Altstetter, C. J. and Tortorelli, P. F.,** Argon ion surface erosion of niobium, *J. Nucl. Materials*, 63, 235, 1976, and references therein.
109. **Barnett, S. A., Bajor, G., and Greene, J. E.,** Growth of high quality epitaxial GaAs films by sputter deposition, *Appl. Phys. Letters*, 37, 734, 1980.
110. **Vossen, J. L.,** Contamination in films sputtered from hot-pressed targets, *J. Vac. Sci. Technol.*, 8, 751, 1971.
111. **Gulbransen, E. A. and Andrew, K. F.,** Kinetics of the reactions of titanium with O_2, N_2, and H_2, *AIME Trans.*, 185, 741, 1949.
112. **Kyle, M. L., Pierce, R. D., Coleman, L. F., and Arntzen, J. D.,** Removal of N_2 from Ar with a titanium metal sponge, *Ind. Engr. Chem. Process Design*, 7, 447, 1968.
113. **Gibbs, D. S., Svec, H. J., and Harrington, R. E.,** Purification of the rare gases, *Ind. Engr. Chem.*, 48, 289, 1956.
114. **Maissel, L. I.,** The deposition of thin films by cathode sputtering, in *Physics of Thin Films*, Vol. 3, Hass, G., and Thun, R. E., Eds., Academic Press, New York, 1966, 61.
115. **Maissel, L. I.,** Application of sputtering to the deposition of films, in *Handbook of Thin Film Technology*, Maissel, L. I. and Glang, R., Eds., Mc-Graw Hill, New York, 1970, chap. 4.
116. **Vossen, J. L.,** Control of film properties by rf sputtering techniques, *J. Vac. Sci. Technol.*, 8, S12, 1971.
117. **Vossen, J. L. and Cuomo, J. J.,** Glow discharge sputter deposition, in *Thin Film Processes*, Vossen, J. L. and Kern, W., Eds., Academic Press, New York, 1978, 11.
118. **Chapman, B.,** *Glow Discharge Processes*, John Wiley and Sons, New York, 1980.
119. **Harper, J. M. E.,** Ion beam deposition in *Thin Film Processes*, Vossen, J. L. and Kern, W., Eds., Academic Press, New York, 1978, 175.
120. **Davis, W. D. and Vanderslice, T. A.,** Ion energies at the cathode of a glow discharge, *Phys. Rev.*, 131, 219, 1963.
121. **Houston, J. E. and Uhl, J. E.,** A characterization of the ionic species incident on the cathode in a glow discharge, Sandia Report Sc-RR-71-0122, 1971.
122. **Tsui, R. T. C.,** Calculation of ion bombarding energy and its distribution in rf sputtering, *Phys. Rev.*, 168, 107, 1968.
123. **Koenig, H. R. and Maissel, L. I.,** Application of rf discharges to sputtering, *IBM J. Res. Dev.*, 14, 168, 1970.
124. **Coburn, J. W. and Kay, E.,** Positive-ion bombardment of substrates in rf diode glow discharge sputtering, *J. Appl. Phys.*, 43, 4965, 1972.
125. **Westwood, W. D. and Boynton, R. J.,** Analysis of sputtering discharge by optical and mass spectrometry. I. Platinum and tantalum sputtered in argon, *J. Appl. Phys.*, 44, 2610, 1973.
126. **Westwood, W. D.,** Analysis of sputtering discharge by optical and mass spectrometry. II. Platinum and tantalum sputtered in argon/nitrogen mixtures, *J. Appl. Phys.*, 44, 2419, 1973.

127. **Greene, J. E., Sequede-Osorio, F., and Natarajan, B. R.,** Glow discharge optical spectroscopy for microvolume elemental analysis, *J. Appl. Phys.*, 46, 2701, 1975.
128. **Greene, J. E.,** Optical spectroscopy for diagnostics and process control during glow discharge, *J. Vac. Sci. Technol.*, 15, 1718, 1978.
129. **Houston, J. E. and Bland, R. D.,** Relationship between sputter cleaning parameters and surface contaminants, *J. Appl. Phys.*, 44, 2504, 1973.
130. **Thornton, J. A. and Penfold, A. S.,** Cylindrical magnetron sputtering, in *Thin Film Processes*, Vossen, J. L., and Kern, W., Eds., Academic Press, New York, 1978, 76.
131. **Fraser, D. B.,** The sputter and S-gun magnetrons, in *Thin Film Processes*, Vossen, J. L., and Kern, W., Eds., Academic Press, New York, 1978, 115.
132. **Waits, R. K.,** Planar magnetron sputtering, in *Thin Film Processes*, Vossen, J. L., and Kern, W., Eds., Academic Press, New York, 1978, 131.
133. See, for example, **Chopra, K. L., Randlett, M. R., and Duff, R. H.,** Face-centered cubic modification in sputtered films of tantalum, molybdenum, tungsten, thenium, hafnium and zirconium, *Philos. Mag.*, 16, 261, 1967.
134. **von Ardenne, M.,** Tabellen der Elektronenphysik, Ionenphysik, und Ubermicroskopie, Dtsch. Verlag Wiss., Berlin, 1956, 554.
135. **Kaufman, H. R.,** Technology of electron-bombardment ion thrusters, *Adv. Electron. Electron Phys.*, 36, 265, 1974.
136. **Reader, P. D. and Kaufman, H. R.,** Optimization of an electron-bombardment ion source for ion machining applications, *J. Vac. Sci. Technol.*, 12, 1344, 1975.
137. Ion Tech, Inc., Fort Collins, Colorado.
138. **Barnett, S. A. and Greene, J. E.,** unpublished.
139. **Eltoukhy, A. H. and Greene, J. E.,** Growth and electrical properties of sputter-deposited single crystal GaSb films on GaAs substrates, *J. Appl. Phys.*, 50, 6396, 1979.
140. **Vossen, J. L.,** Transparent conducting films, in *Physics of Thin Films*, Vol. 9, Hass, G., Francombe, M. H., and Hoffman, R. W., Eds., Academic Press, New York, 1977, 1.
141. **Wickersham, C. E. and Greene, J. E.,** The effect of substrate bias on the electrical and optical properties of In_2O_3 films grown by rf sputtering, *Phys. Stat. Sol. (a)*, 47, 329, 1978.
142. **Ohhata, Y., Shinoki, F., and Yoshida, S.,** Optical properties of rf reactive sputtered tin-doped In_2O_3 films, *Thin Solid Films*, 59, 255, 1979.
143. **Miyata, N., Miyake, K., Koga, K., and Fukushima, T.,** Transparent conducting cadmium-tin oxide films deposited by rf sputtering from a $CdO\text{-}SnO_2$ target, *J. Electrochem. Soc.*, 127, 918, 1980.
144. **Natarajan, B. R., Eltoukhy, A. H., Greene, J. E., and Barr, T. L.,** Mechanisms of the reactive sputtering of In I. Growth of InN in mixed $Ar\text{-}N_2$ discharges, *Thin Solid Films*, 69, 201, 1980.
145. **Berak, J. M. and Quinn, D. J.,** Utilization of a subliming solid (arsenic) in rf reactive sputtering, *J. Vac. Sci. Technol.*, 13, 609.
146. **Fraser, D. B. and Melchoir, H.,** Sputter-deposited CdS films with high photoconductivity through film thickness, *J. Appl. Phys.*, 43, 3120, 1972.
147. **Westwood, W. D. and Ingrey, S. J.,** Fabrication of optical wave guides by ion-beam sputtering, *J. Vac. Sci. Technol.*, 13, 104, 1976.
148. **Weissmantel, C.,** Reactive film preparation, *Thin Solid Films*, 32, 11, 1976.
149. **Natarajan, B. R., Eltoukhy, A. H., Greene, J. E., and Barr, T. L.,** Mechanisms of the reactive sputtering of In, Part 2: Growth of indium oxynitride in mixed $N_2\text{-}O_2$ discharges, *Thin Solid Films*, 69, 217, 1980.
150. **Eltoukhy, A. H., Natarajan, B. R., Greene, J. E., and Barr, T. L.,** Mechanisms of the reaction sputtering of IN, Part 3: A general phenomenological model for reactive sputtering, *Thin Solid Films*, 69, 229, 1980.
151. **Hovel H. J. and Cuomo, J. J.,** Electrical and optical properties of rf-sputtered GaN and InN, *Appl. Phys. Letters*, 20, 71, 1972.
152. **Greene, J. E., Barnett, S. A., Cadien, K. C., and Ray, M. A.,** Growth of single crystal GaAs and metastable $(GaSb)_{1-x}$ alloys by sputter deposition: ion-surface interaction effects, *J. Cryst. Growth*, 56, 389, 1982.
153. **Winters, H. F., Raimondi, D. L., and Horne, D. E.,** Proposed model for the composition of sputtered multicomponent thin films, *J. Appl. Phys.*, 40, 2996, 1969.
154. **Bolker, B. F. T., Sidles, P. H., and Danielson, G. C.,** Variable composition thin films in ternary chalcogenide systems by rf cosputtering, *J. Vac. Sci. Technol.*, 12, 114, 1975.
155. **Heiman, N., Kazama, N., Kyser, D. F., and Muikiewiez, V. J.,** Effects of substrate bias and annealing on the properties of amorphous alloy films of Gd-Co, Gd-Fe, and Gd-Co-X (X = Mo, Cu, Au), *J. Appl. Phys.*, 49, 366, 1978.
156. **Cuomo, J. J. and Gambino, R. J.,** Influence of sputtering parameters on the composition of multi-component films, *J. Vac. Soc. Technol.*, 12, 79, 1975.

157. **Rivaud, L, Romano, L. T., Barnett, S. A., and Greene, J. E.,** unpublished.
158. **Narusawa, T., Shimizu, S., and Komiya, S.,** Simultaneous RHEED-AES-QMS study on epitaxial Si film growth on Si (111) and sapphire (1102) surfaces by partially ionized vapor deposition, *J. Vac. Sci. Technol.*, 16, 366, 1979.
159. **Nowicki, R. S., Buckley, W. D., Mackintosh, W. D., and Mitchell, I. V.,** Effects of deposition parameters on properties of rf sputtered molybdenum films, *J. Vac. Sci. Technol.*, 11, 675, 1974.
160. **Cadien, K. C., Eltoukhy, A. H., and Greene, J. E.,** Growth of single crystal metastable semiconducting $(GaSb)_{1-x}$ Ge_x films, *Appl. Phys. Letters*, 38, 773, 1981.
161. **Blachman, A. G.,** dc bias-sputtered aluminum films, *J. Vac. Sci. Technol.*, 10, 299, 1973.
162. **Zilko, J. L. and Greene, J. E.,** Growth and phase stability of epitaxial metastable $InSb_{1-x}Bi_x$ films on GaAs, Part 1: Crystal growth, *J. Appl. Phys.*, 51, 1549, 1980.
163. **Bland, R. D., Kominiak, G. J., and Mattox, D. M.,** Effect of ion bombardment during deposition on thick metal and ceramic deposits, *J. Vac. Sci. Technol.*, 11, 671, 1974.
164. **Pan, A. and Greene, J. E.,** Residual compressive stress in sputter deposited TiC films on steel substrates, *Thin Solid Films*, 78, 25, 1981.
165. **Hanak, J. J.,** The "multiple-sample concept" in materials research: synthesis, compositional analysis and testing of entire multicomponent systems, *J. Materl. Sci.*, 5, 964, 1970.
166. **Hanak, J. J., Lehman, H. W., and Wehner, R. K.,** Calculation of deposition profiles and compositional analysis of cosputtered films, *J. Appl. Phys.*, 43, 1666, 1972.
167. **Greene, J. E., Wickersham, C. E., and Zilko, J. L.,** Growth of $In_{1-x}Ga_xSb$ and $In_{1-x}Al_xSb$ films by multi-target rf sputtering, *Thin Solid Films*, 32, 51, 1976.
168. **Greene, J. E., Wickersham, C. E., and Zilko, J. L.,** Epitaxial growth of $In_{1-x}Ga_xSb$ thin films by multitarget rf sputtering, *J. Appl. Phys.*, 47, 2289, 1976.
169. **Wickersham, C. E. and Greene, J. E.,** Multitarget sputtering using decoupled plasmas, *J. Appl. Phys.*, 47, 4734, 1976.
170. **Eltoukhy, A. H. and Greene, J. E.,** Ion bombardment enhanced diffusion during the growth of sputtered superlattice thin films, *Appl. Phys. Letters*, 33, 343, 1978.
171. **Eltoukhy, A. H. and Greene, J. E.,** Compositionally modulated sputtered InSb/GaSb superlattices: Crystal growth and interlayer diffusion, *J. Appl. Phys.*, 50, 505, 1979.
172. **Nowicki, R. S.,** The rf diode co-deposition of refractorymetal silicides, *Sol. St. Technol.*, Nov., 1980, 95.
173. **Ball, D. J.,** Plasma diagnostics and energy transport of a dc discharge used for sputtering, *J. Appl. Phys.*, 43, 3047, 1972.
174. **Chapman, B. N. Downer, D., and Guimaraes, L. J. M.,** Electron effects in sputtering and co-sputtering, *J. Appl. Phys.*, 45, 2115, 1974.
175. **Lau, S. S., Mills, R. H., and Muth, D. G.,** Temperature rise during film deposition by rf and dc sputtering, *J. Vac. Sci. Technol.*, 9, 1196, 1972.
176. **Barnett, S. A. and Greene, J. E.,** unpublished.
177. **Stirling, D. J.,** electron bombardment induced changes in the growth and epitaxy of evaporated gold films, *Appl. Phys. Letters*, 9, 326, 1966.
178. **Palmberg, P. W., Rhodin, T. N., and Todd, C. J.,** Low energy electron diffraction studies of epitaxial growth of silver and gold in ultra-high vacuum, *Appl. Phys. Letters*, 10, 122, 1967.
179. **Palmberg, P. W., Todd, C. T., and Rhodin, T. N.,** Role of surface defects in the epitaxial growth of some fcc metals on potassium chloride cleaved in ultra-high vacuum, *J. Appl. Phys.*, 39, 4650, 1968.
180. **Jordan, M. R. and Stirland, D. J.,** Changes in epitaxy produced by electron bombardment, *Thin Solid Films*, 8, 221, 1971.
181. **Lord, D. G. and Prutton, M.,** Electrons and the epitaxial growth of metals on alkaki halides, *Thin Solid Films*, 21, 341, 1974.
182. **Shimaoka, G.,** Modifications of epitaxy in evaporated films by electric charge effects, *J. Cryst. Growth*, 31, 92, 1975.
183. **Namba, Y. and Nagai, K.,** Epitaxy of Ag on NaCl deposited by ion deposition, *Japn. J. Appl. Phys.*, 15, 377, 1976.
184. **Chapman, B. N. and Campbell, D. S.,** Condensation of high-energy atomic beams, *J. Phys. C.*, 2, 200, 1969.
185. **Adamov, M., Perovic, B., and Nenadovic, T.,** Electrical and structural properties of thin gold films obtained by vacuum evaporation and sputtering, *Thin Solid Films*, 24, 89, 1974.
186. **Ueda, R.,** Film growth of metals and semiconductors with ionized beams and surface imperfections, *Thin Solid Films*, 39, 25, 1976.
187. **Bykov, Yu. V., Guseva, M. B., Kevedo, Kh., and Adbrashitova, D. Kh.,** Epitaxial gold films during ion bombardment, *Bull. Akad. Nauk. SSSR*, 41, 135, 1977.
188. **Krikorian, E. and Sneed, R. J.,** Nucleation, growth, and transformation of amorphous and crystalline solids condensing from the gas phase, *Astrophys. Space Science*, 65, 129, 1979.

189. **Ueda, R.**, Synthesis and epitaxial growth of CdTe films by neutral and ionized beams, *J. Cryst. Growth*, 31, 333, 1975.
190. **Namba, Y. and Mori, T.**, Epitaxial growth of ZnTe on NaCl by ion deposition, *Thin Solid Films*, 39, 119, 1976.
191. **Lane, G. E. and Anderson, J. C.**, The nucleation and initial growth of gold films deposited onto sodium chloride by ion beam sputtering, *Thin Solid Films*, 26, 5, 1975.
192. **Lane, G. E. and Anderson, J. C.**, Features of the initial growth of gold films deposited on rock-salt substrates by ion beam sputtering, *Thin Solid Films*, 57, 277, 1979.
193. **Marinov, M.**, Effect of ion bombardment on the initial stages of thin film growth, *Thin Solid Films*, 46, 267, 1977.
194. **Shawki, G. S. A., El-Sherbiny, M. G., and Salem, F. B.**, Nucleation and interface formation in thin films, *Thin Solid Films*, 75, 29, 1981.
195. **Bovey, P. E.**, The effect of arrival energy on the properties of gold films, *Vacuum*, 19, 497, 1969.
196. **Cornely, R. H., Mumtaz, A., and Fuschillo, N.**, Nucleation and growth of rf triode sputtered gold films, *J. Vac. Sci. Technol.*, 12, 693, 1975.
197. **Babaev, V. O., Bykov, Ju. V., and Guseva, M. B.**, Effect of ion irradiation on the formation, structure and properties of thin metal films, *Thin Solid Films*, 38, 1, 1976.
198. See discussion in reference 186.
199. **Aleksandrove, L. N., Lutovich, A. S., and Beloresets, E. D.**, The mechanism of silicon epitaxial layer growth from ion-molecular beams, *Phys. Stat. Sol. (a)*, 54, 463, 1979.
200. **Shimizu, S. and Komiya, S.**, Effects of Ga and Si ionization of the growth of Ga doped Si MBE, *J. Vac. Sci. Technol.*, 18, 765, 1981.
201. **Pchelyakov, O. P., Lovyagin, R. N., Krivorotov, E. A., Toropov, A. I., Aleksandrov, L. N., and Stenin, S. I.**, Silicon homoepitaxy with ion sputtering, I. Mechanism of growth, *Phys. Stat. Sol. (a)*, 17, 339, 1973.
202. **Aleksandrov, L. N. and Lovyagin, R. N.**, Homoepitaxial growth of silicon films by ion sputtering, *Japn. J. Appl. Phys.*, Suppl. 2, Pt. 1, 609, 1974, Proc. 6th Internatl. Vac. Congr., Kyoto, Japan.
203. **Aleksandrov, L. N. and Lovyagin, R. N.**, Step motion of the growth surface in the initial stage of semiconductor film epitaxy with ion sputtering, *Thin Solid, Films*, 20, 1, 1974.
204. **Chopra, K. L.** Influence of electric field on the growth of thin films, *J. Appl. Phys.*, 37, 2249, 1966.
205. **Gunnier, A.**, *X-ray Diffraction in Crystals, Imperfect Crystals, and Amorphous Bodies*, translated by P. Larrian and D. Saint Marie Lorrian, W. H. Freeman and Co., San Francisco, 1963, 279.
206. **Cadien, K. C., Eltoukhy, A. H., and Greene, J. E.**, Growth and thermal stability of single crystal metastable semiconducting $(GaSb)_{1-x}Ge_x$ films, *Vacuum*, 31, 253, 1981.
207. **Tsaur, B. Y., Mayer, J. W., and Tu, K. N.**, Ion-beam induced metastable Pt_2Si_3 phase: I. Formation, structure, and properties, *J. Appl. Phys.*, 51, 5326, 1980.
208. **Tsaur, B. Y., Mayer, J. W., Graczyk, J. F., and Tu, K. N.**, Ion-beam induced metastable Pt_2Si_3 phase: II. Kinetics and morphology, *J. Appl. Phys.*, 51, 5334, 1980.
209. **Tsuar, B. Y., Lau, S. S., and Mayer, J. W.**, Continuous series of Ag-Cu solid solutions formed by ion beam-mixing, *Appl. Phys. Letters*, 36, 823, 1980.
210. **Winters, H. F.**, Ionic adsorption and dissociation cross-section for nitrogen, *J. Chem. Phys.*, 44, 1472, 1966.
211. **Rivaud, L., Ward, I. D., Eltoukhy, A. H., and Greene, J. E.**, Enhanced diffusion and precipitation in Cu: In alloys due to low energy ion bombardment, *Surf. Sci.*, 102, 610, 1981.
212. **Rivaud, L, Eltoukhy, A. H., and Greene, J. E.**, Low energy ion bombardment enhanced diffusion, segregation, and phase transformations in Cu: In alloys, *Rad. Eff.*, 61, 83, 1982.
213. **Winters, H. F. and Kay, E.**, Gas incorporation into sputtered films, *J. Appl. Phys.*, 38, 3928, 1967.
214. **Lee, W. W. Y. and Oblas, D.**, Argon entrapment in metals films by dc triode sputtering, *J. Appl. Phys.*, 46, 1728, 1975.
215. **Cuomo, J. J. and Gambino, R. J.**, Incorporation of rare gases in sputtered amorphous metal films, *J. Vac. Sci. Technol.*, 14, 152, 1977.
216. **Andersen, H. H. and Sigmund, P.**, Defect distributions in channeling experiments, *Nucl. Instr. Methods*, 38, 238, 1965.
217. **Barnett, S. A. and Greene, J. E.**, unpublished result.
218. **Naganuma, M. and Takahashi, K.**, Ionized Zn doping of GaAs molecular beam epitaxial films, *Appl. Phys. Letters*, 27, 342, 1975.
219. **Matsunaga, N., Suzuki, T., and Takahaski, J.**, Ionized beam doping in molecular beam epitaxy of GaAs and $Al_xGa_{1-x}As$, *J. Appl. Phys.*, 49, 5710, 1978.
220. **Bean, J. C. and Dingle, R.**, Luminescent p-GaAs grown by zinc ion doped MBE, *Appl. Phys. Letters*, 35, 925, 1979.
221. **Itah, T., Nakamura, T., Muromachi, M., and Sugiyama, T.**, Antimony concentrations in silicon epitaxial layer formed by partially ionized vapor deposition, *Japan. J. Appl. Phys.*, 15, 1145, 1976.

222. **Ota, Y.,** Silicon molecular beam epitaxy with simultaneous ion implant doping, *J. Appl. Phys.*, 52, 1102, 1980.
223. **Francombe, M. H.,** Preparation and properties of sputtered films, *Trans. 10th Nat. Vacuum Symp.*, 1968, p. 316.
224. **Francombe, M. H.,** The preparation of epitaxial films by evaporation and cathodic sputtering, in *The Use of Thin Films in Physical Investigations*, Anderson, J. C., Ed., Academic Press, New York, 1966, 29.
225. **Francombe, M. H.,** Growth of epitaxial films by sputtering, in *Epitaxial Growth*, Matthews, J. W., Ed., Academic Press, New York, 1971, 109.
226. **Greene, J. E.,** Crystal growth by sputtering, in *Handbook of Semiconductors*, Vol. III, Keller, S. P., Ed., North Holland Publishing Co., Amsterdam, 1980, 499.
227. **Greene, J. E. and Eltoukhy, A. H.,** Semiconductor crystal growth by sputter deposition, *Surf. Interface Analysis*, 3, 34, 1981.
228. **Krikorian, E. and Sneed, R. J.,** Deposition parameters affecting epitaxial growth of single crystal films, *Trans. 10th Nat. Vacuum Symp.*, New York, 1963, 368.
229. **Krikorian, E.,** sputtering parameters affecting epitaxial growth of semiconductor single crystal films in *Single Crystal Films*, Francombe, M. H., and Sato, H., Eds., Pergamon Press, Oxford, 1964, 113.
230. **Wolsky, S. P., Piwkowski, T. R., and Wallis, G.,** Low pressure sputtered germanium films, *J. Vac. Sci. Technol.*, 2, 97, 1965.
231. **Haq, K. E.,** Deposition of germanium films by sputtering, *J. Electrochem. Soc.*, 112, 500, 1965.
232. **Krikorian, E. and Sneed, R. J.,** Epitaxial deposition of germanium by both sputtering and evaporation, *J. Appl. Phys.*, 37, 3665, 1966.
233. **Khan, J. T.,** Low temperature epitaxy of Ge films by sputter deposition, *J. Appl. Phys.*, 44, 14, 1973.
234. **Adamsky, R. F.,** Effect of deposition parameters on the crystallinity of evaporated germanium films, *J. Appl. Phys.*, 40, 4301, 1969.
235. **Layton, C. K. and Cross, K. B.,** The growth of epitaxial germanium films by triode sputtering, *Thin Solid Films*, 1, 169, 1977.
236. **Cadien, K. C. and Greene, J. E.,** Crystal growth and controled doping of epitaxial Ge films on (100) GaAs sputter deposition, *J. Crystal Growth*, in press.
237. **Sze, S. M.,** *Physics of Semiconductor Devices*, John Wiley and Sons, New York, 1969, 40.
238. **Unvala, G. A. and Pearman, K.,** Growth of epitaxial silicon layers by ion beam sputtering, *J. Mat. Sci.*, 5, 1016, 1970.
239. **Weissmantel, C., Fielder, O., Hecht, G., and Reisse, G.,** Ion beam sputtering and its application for the deposition of semiconducting films, *Thin Solid Films*, 13, 359, 1972.
240. **Weissmantel C.,** Ion beam utilization for etching and film deposition, *Vide*, 183, 107, 1976.
241. **Hinneberg, H. J., Weidner, M., Hect, G., and Weissmantel, C.,** Electrical properties of ion beam sputtered silicon layers on spinel, *Thin Solid Films*, 33, 25, 1976.
242. **El-Dessouki, M. S. and Weissmantel,** Photoelectic, optical, and structure properties of ion beam sputtered silicon films on spinel, *Proc. 7th Internat. Vacuum Congr.*, Vienna, 1977, 1955.
243. **Harmon, R. V., Tvarozek, O., Vanek, O., Kempny, M., and Liday, J.,** rf sputtered silicon films on sapphire, *Thin Solid Films*, 32, 55, 1976.
244. **Ito, K.,** Preparation of Ge-Si epitaxial alloys by sputtering, *J. Cryst. Growth*, 45, 340, 1978.
245. **Aleksandrov, L. N., Lovagin, R. N., Pchelyakov, O. P., and Stenin, S. I.,** Heteroepitaxy of germanium thin films on silicon byion sputtering, *J. Cryst. Growth*, 24/25, 298, 1974.
246. **Bajor, G., Cadien, K. C., Ray, M., Greene, J. E., and Vijayakumar, P. S.,** The growth of high quality epitaxial Ge films on (100)Si by sputter deposition, *Appl. Phys. Letters*, 40, 696, 1982.
247. **Gunther, K.,** Interfacial and condensation processes occurring with multicomponent vapors, in *The Use of Thin Films for Physical Investigations*, Anderson, J. C., Ed., Academic Press, New York, 1966, 213.
248. See, for example, **Cho, A. Y. and Arthur, J. R.,** Molecular beam epitaxy, *Prog. Sol. St. Chem.*, 20, 157, 1975.
249. **Francombe, M. H., Flood, J. J., and Turner, T. L.,** *5th Internat. Congr. electron Microscopy*, Vol. I., Philadelphia, 1962, DD-8.
250. **Yurasova, V. E., Levykina, L. N., and Efremenkova, V. M.,** Preparation of thin intermetallic compound films by the cathode sputtering method, *Sov. Phys. Sol. State St.*, 7, 2332, 1966.
251. **Kahn, T. H.,** Epitaxial growth on indium antimonide films as studied by in-situ electron diffraction, *Surface Sci.*, 9, 306, 1968.
252. **Cervenak, J., Zivakova, A., and Buch, J.,** Structure and electrical properties of Insb thin films prepared by plasmatic sputtering, *Czech. J. Phys.*, B20, 84, 1970.
253. **Jachimowski, M. and Kusier, E.,** Recrystallization of InSb thin films obtained by cathode sputtering, *Thin Solid Films*, 24, 151, 1974.
254. **Greene, J. E. and Wickersham, C. E.,** Structure and electrical characteristics of InSb thin films grown by rf sputtering, *J. Appl. Phys.*, 47, 3630, 1976.

255. **Bajor, G., Barnett, S. A., Klinger, R. E., and Greene, J. E.,** Determination of concentrations and ionization energies of imperfections in degenerate InSb films, *Thin Solid Films,* 59, 183, 1979.
256. **Barnett, S. A., Bajor, G., Eltoukhy, A. H., and Greene, J. E.,** to be published.
257. **Eltoukhy, A. H. and Greene, J. E.,** unpublished.
258. **Eltoukhy, A. H.,** Ph.D. thesis, Department of Metallurgy, University of Illinois, Urbana, 1978.
259. **Jachimowski, M. and Data, A.,** dc sputtered $Al_xIn_{1-x}Sb$ films, *Thin Solid Films,* 48, L15, 1978.
260. **Jha, K. N. and Korgaonkar, A. V.,** Electrical properties of dc sputtered InAs thin films, *Thin Solid Films,* 9, 133, 1971.
261. **Szczyrbowski, J., Czapla, A., and Jachimowski, M.,** dc sputtering of thin indium arsenide films, *Thin Solid Films,* 42, 193, 1977.
262. **Molnar, B., Flood, J. J., and Francombe, M. H.,** Fibered and Epitaxial growth in sputtered films of GaAs, *J. Appl. Phys.,* 35, 3554, 1965.
263. **Evanns, T. and Noreika, A. J.,** Effect of gaseous environment on the structure of sputtered GaAs films on NaCl substrates, *Phil. Mag.,* 23, 717, 1966.
264. **Bunton, G. V. and Day, S. C. M.,** Epitaxial thin films of ZnS and GaAs prepared by rf sputtering on NaCl substrates, *Thin Solid Films,* 20, 22, 1972.
265. **Ray, M., Barnett, S. A., Chen, Haydn, and Greene, J. E.,** unpublished.
266. **Illegems, M., Dingle, R., and Rupp Jr., L. W.,** Optical and electrical properties of Mn-doped GaAs grown by molecular beam, epitaxy, *J. Appl. Phys.,* 46, 3059, 1975.
267. **Rosztoczy, F. E., Ermanis, F., Hayashi, I., and Schwartz, B.,** Germanium doped GaAs, *J. Appl. Phys.,* 41, 264, 1970.
268. **Vilms, J. and Garrett, J. P.,** The growth and properties of LPe and GaAs, *Sol. St. Electronics,* 15, 443, 1972.
269. **Rutz, R., Harris, E. P., and Cuomo, J. J.,** *IBM J. Res. Dev.,* 27, 61, 1973.
270. **Duchene, J.,** Radiofrequency reactive sputtering for deposition of aluminum nitride thin films, *Thin Solid Films,* 8, 69, 1971.
271. **Puychevrier, N. and Monoret, M.,** Synthesis of III-V semiconductor nitrides by reactive cathodic sputtering, *Thin Solid Films,* 36, 141, 1976.
272. **Favennec, P. N., Henry, L., Janicki, T., and Salvi, M.,** Protection due GaAs, $Ga_{1-x}Al_xAs$, et $GaAs_{1-x}P_x$, par due nitrure d'aluminum depose par pulverisation reactive, *Thin Solid Films,* 47, 327, 1977.
273. **Noreika, A. J., Francombe, M. H., and Zeitman, S. A.,** Dielectric properties of reactively sputtered films of aluminum nitride, *J. Vac. Sci. Technol.,* 6, 194, 1969.
274. **Shuskus, A. J., Reeder, T. M., and Paradis, E. L.,** rf sputtered aluminum nitride films on sapphire, *Appl. Phys. Letters,* 24, 155, 1974.
275. **Vesely, J. C., Shatzkes, M., and Burkhardt, P. T.,** Space-charge-limited current flow in gallium nitride thin films, *Phys. Rev. B,* 10, 582, 1974.
276. **Sosniak, J.,** Gallium phosphide films deposited by sputtering, *J. Vac. Sci. Technol.,* 7, 110, 1970.
277. **Starosta, K., Zellinka, J., Berkova, D., and Kohout, J.,** rf sputtering of gallium phosphide thin films, *Thin Solid Films,* 61, 241, 1979.
278. **Hickernell, F. S.,** dc triode sputtered zinc oxide surface elastic wave transducers, *J. Appl. Phys.,* 44, 1061, 1973.
279. **Khuri-Yakub, B. S., Kino, G. S., and Galle, P.,** Studies of the optimum conditions for growth of rf-sputtered ZnO films, *J. Appl. Phys.,* 46, 3266, 1975.
280. **Ohji, K., Tohda, T., Wasa, K., and Hayakawa, S.,** Highly oriented ZnO films by rf sputtering of hemispherical electrode system, *J. Appl. Phys.,* 47, 1726, 1976.
281. **Paradis, E. L. and Shuskus, A. J.,** rf sputtered epitaxial ZnO films on sapphire for integrated optics, *Thin Solid Films,* 38, 131, 1976.
282. **Mitsuyu, T., Ono, S., and Wasa, K.,** Structure and SAW properties of rf-sputtered single-crystal films of ZnO on sapphire, *J. Appl. Phys.,* 52, 2464, 1980.
283. **Ambersley, M. D. and Pitt, C. W.,** Piezoelectric ZnO transducers produced by rf magnetron sputtering, *Thin Solid Films,* 80, 183, 1981.
284. **Fritsche, H.,** Der einfluss von gelostein sauerstoff auf die elektrische leitfahigkeit von zinkoxyd, *Z. Phys.,* 133, 422, 1952.
285. **Raimondi, D. L. and Kay, E.,** High resistivity transparent ZnO thin films, *J. Vac. Sci. Technol.,* 7, 96, 1970.
286. **Rozgoni, G. A. and Polito, W. J.,** Preparation of ZnO thin films by sputtering of the compound in oxygen and argon, *Appl. Phys. Letters,* 8, 220, 1966.
287. **Rozgonyi, G. A. and Polito, J. R.,** Epitaxial thin films of ZnO on CdS and sapphire, *J. Vac. Sci. Technol.,* 6, 115, 1969.
288. **Foster, N. F.,** Crystallographic orientation of zinc oxide films deposited by triode sputtering, *J. Vac. Sci. Technol.,* 6, 111, 1969.

289. **Maniv, S. and Zangvil, A.,** Controlled texture of reactively rf sputtered ZnO thin films, *J. Appl. Phys.*, 49, 2787, 1978.
290. **Lad, R. J., Funkenbush, P. D., and Aita, C. R.,** Post deposition annealing behavior of rf sputtered ZnO films, *J. Vac. Sci. Technol.*, 17, 808, 1980.
291. **Ohji, K., Yamazaki, O., Wasa, K., and Hayakawa, S.,** New sputtering system for manufacturing ZnO thin film SAW devices, *J. Vac. Sci. Technol.*, 15, 1601, 1978.
292. **Hada, T., Wasa, K., and Hayakawa, S.,** Structures and electrical properties of zinc oxide films prepared by low pressure sputtering system, *Thin Solid Films*, 7, 135, 1971.
293. **Hata, T., Minamikawa, T., Morimoto, O., and Hada, T.,** dc reactive magnetron sputtered ZnO films, *J. Cryst. Growth*, 47, 171, 1979.
294. **Shiosaki, T., Ohnishi, S., Murakami, Y., and Kawabata, A.,** High rate epitaxial growth of ZnO films on sapphire by planar magnetron rf sputtering system, *J. Cryst. Growth*, 45, 364, 1978.
295. **Glew, R. W.,** Cadmium selenide sputtered films, *Thin Solid Films*, 46, 59, 1977.
296. **Tanaka, K.,** Photoconductivity of CdSe films prepared by a vapor evaporating reactive sputtering method, *Japn. J. Appl. Phys.*, 9, 1070, 1970.
297. **Lehmann, H. W. and Wildmer, R.,** Radio frequency sputtering of CdSe films, *Thin Solid Films*, 33, 301, 1976.
298. **Helwig, G. and Konig, H.,** Uber die herstellulng von lichtempfindlilchen cadmiumsulfidschichten durch kathodenzerstaubung, *Z. Angew. Phys.*, 7, 323, 1955.
299. **Dresner, J. and Shallcross, F. V.,** Rectification and space-charge-limited currents in CdS films, *Sol. Stat. Electron.*, 5, 205, 1962.
300. **Lakshamanan, T. K. and Mitchell, J. M.,** Some properties of sputtered sulphide films, *Trans. 10th American Vacuum Soc. Symp.*, 1963, p. 335.
301. **Lichtensteiger, M., Lagnado, I., and Gatos, H. C.,** p-type cadmium sulphide crystalline films, *Appl. Phys. Letters*, 15, 418, 1969.
302. **Durand, S., Bugnet, P., Deforges, J., and Onderdelinden, D.,** Precision measurements of the angular and temperature dependence of sputtering, *Radiat. Eff.*, 14, 93, 1972.
303. **Boronkay, S., Cassanhiol, B., and Deforges, J.,** Couches minces de CdS photosensibles par pulverisation cathodique rf reactive, *Vide*, 32, 94, 1977.
304. **Durand, S., Bugnet, P., Deforges, J., and Batailler, G.,** Application de la pulverisation cathodique reactive a la fabrication de CdS photosensible, *Thin Solid Films*, 11, 237, 1971.
305. **Takeuchi, M., Sakagawa, Y., and Nagasaka, H.,** Photoconduction and photovoltaic effects in sputtered CdS films, *Thin Solid Films*, 33, 89, 1976.
306. **Clarke, J. R. and Greene, J. E.,** Polycrystalline CdS films with large photoconductive gain grown by reactive sputtering, *J. Vac. Sci., Technol.*, 18, 382, 1981.
307. **Nakada, T.,** Growth and structure of rf sputtered HgS films on NaCl, *J. Appl. Phys.*, 48, 3405, 1977.
308. **Nakada, T. and Kunioka, A.,** Effect of potassium of crystal modification of rf sputtered HgS films, *Japn. J. Appl. Phys.*, 16, 1045, 1977.
309. **Nakada, T. and Kunioka, A.,** Growth and properties of sputter deposited α-HgS films in Hg vapor, *Japn. J. Appl. Phys.*, 19, 845, 1980.
310. **Jones, P. L., Moore, D., and Smith, D. C. A.,** A technique for the growth of single crystal films of zinc sulphide on (100) gallium arsenide by radio frequency sputtering, *J. Phys. E. Sci. Instr.*, 9, 312, 1976.
311. **Schonbrodt, L. and Reichett, K.,** Preparation of ZnS films by reactive sputtering and their investigation by electron microscopy and Rutherford backscattering, *Thin Solid Films*, 81, 45, 1981.
312. **Durand, S., Bulgnet, P., and Deforges, J.,** Pulverisation cathodique reactive du sulfure de zinc active au cuivre et au chlore, *Vide*, 30, 8, 1975.
313. **Deforges, J., Durand, S., and Bugnet, P.,** Variations du pourcentage de ZnS dans des solutions solides de An_1- Cd_xS obtenues par pulverisation cathodique reactive, *Thin Solid Films*, 18, 231, 1973.
314. **Deforges, J., Cachard, A., and D. Lupin, J. P.,** Etude de solutions solides de composes II-VI obtenues par copulverisation reactive, *Vide*, 32, 26, 1977.
315. **Fraser, D. B.,** Sputter deposited films for display devices, *Thin Solid Films*, 13, 407, 1972.
316. **Valentovic, D., Cervenak, J., Luby, S., Aldea, M. L., and Boila, T.,** Some non-equilibrium phenomena in sputtered CdTe thin films, *Phys. Stat. Sol. A.*, 56, 341, 1979.
317. **Gonzalez-Diaz, G., Rodriguez-Vidal, M., Sanchez-Quesada, F., and Valles-Abarca, J. A.,** Electrode effects in the ac characteristics of thin sputtered CdTe films, *Thin Solid Films*, 58, 67, 1971.
318. **Pawlewicz, W. T., Allen, R. P., Barrus, H. G., and Laegreid, N.,** Structure and properties of sputter-deposited CdTe, *Rev. Phys. Appl.*, 12, 417, 1977.
319. **Zozime, A., Sella, C., and Cohen-Solal, G.,** Sputtering of $Cd_xHg_{1-x}Te$ films in mercury vapor plasma, *Thin Solid Films*, 13, 373, 1972.
320. **Zozime, A., Cohen-Solal, G., and Bailly, F.,** Growth of thin films of $Cd_xHg_{1-x}Te$ solid solutions by cathode sputtering in a mercury vapor plasma, *Thin Solid Films*, 70, 139, 1980.

321. **Cohen-Solal, G., Sella, C., Imhoff, D., and Zozime, A.,** Structure and properties of $Cd_xHg_{1-x}Te$ films, *Japn. J. Appl. Phys.*, Suppl. 2, Pt. 1, 517, 1974.
322. **Cornely, R. H., Suchow, L., Gabara, T., and Diodato, P.,** rf triode-sputtered mercury cadmium telluride thin films, *IEEE Trans. Electron Devices*, D-27, 29, 1980.
323. **Corsi, C.,** $Pb_xSn_{1-x}Te$ layers by rf multicathode sputtering, *Appl. Phys. Letters*, 24, 137, 1974.
324. **Corsi, C.,** $Pb_xSn_{1-x}Te$ layers by rf multicathode sputtering, *J. Appl. Phys.*, 45, 3467, 1974.
325. **Corsi, C., Fainelli, E., Petrocco, G., Vitali, G., Campisano, U., Foti, G., and Rimini, E.,** Single crystal heteroepitaxial growth of $Pb_xSn_{1-x}Te$ films on germanium substrates by rf sputtering, *Thin Solid Films*, 33, 135, 1976.
326. **Krikorian, E., Crisp, M. T., and Sneed, R. J.,** General Dynamics Technical Report AFML-TR-75-63. Available from Air Force Materials Laboratory, Wright Patterson Air Force Base, Ohio.
327. **Francombe, M. H.,** Crystal growth and orientation in sputtered films of bismuth telluride, *Phil. Mag.*, 10, 989, 1964.
328. **Hewig, G. H. and Bloss, W. H.,** Technology of thin film solar cells, *Thin Solid Films*, 45, 1, 1977.
329. **Potter, R. W.,** An electrochemical investigation of the system copper-sulphur, *Econ. Geol.*, 72, 1524, 1977.
330. **Armantrout, G. A., Miller, D. E., Vindelov, K. E., and Brown, T. G.,** Formation of thin Cu_2S (chalcocite) films using reactive sputtering techniques, *J. Vac. Sci. Technol.*, 16, 212, 1979.
331. **Radler, K., Frey, H., Muller, W., Schuller, K. H., and von Wienskowski, J.,** Structural, electrical and optical properties of Cu_xS layers produced by reactive of sputtering, *Thin Solid Films*, 59, 13, 1979.
332. **Jonath, A. D., Anderson, W. W., Thornton, J. A., and Cornog, D. G.,** Copper sulfide films deposited by cylindrical magnetron reactive sputtering, *J. Vac. Sci. Technol.*, 16, 200, 1979.
333. **Hwang, H. L., Sun, C. Y., Leu, C. Y., Cheng, C. L., and Tu, C. C.,** Growth of $CuInS_2$ and its characterization, *Rev. Phys. Appl.*, 13, 745, 1978.
334. **Hwang, H. L., Cheng, C. L., Liu, L. M., Liu, Y. C., and Sun, C. Y.,** Growth and properties of sputter deposited $CuInS_2$ thin films, *Thin Solid Films*, 67, 83, 1980.
335. **Piekoszewski, J., Loferski, J. J., Beulieu, R., Beall, J., Roessler, B., and Shewchun, J.,** Rf sputtered $CuInSe_2$ thin films, *Sol. Energy Mater.*, 2, 363, 1980.
336. **Scholl, F. W. and Cory, E. S.,** Preparation and properties of $ZnGeAs_2$, *Mat. Res. Bull.*, 9, 1511, 1974.
337. **Shah, S. I. and Greene, J. E.,** unpublished.
338. **Jones, H.,** Splat cooling and metastable phases, *Rep. Prog. Phys.*, 36, 1425, 1973.
339. See, for example, **Poate, J. M.,** Metastable alloy formation, *J. Vac. Sci. Technol.*, 15, 1636, 1978.
340. See, for example, articles in *Laser and Electron Beam Processing of Materials*, White, C. W., and Preecy, P. S., Eds., Academic Press, New York, 1980.
341. **Greene, J. E., Cadien, K. C., Lubben, D., Hawkins, G. A., Erikson, G. R., and Clarke, J. R.,** Epitaxial Ge/GaAs heterostructures by scanned CW laser annealing of Ge layers on GaAs, *Appl. Phys. Letters*, 39, 232, 1981.
342. **Noreika, A. J. and Francombe, M. H.,** Preparation of nonequilibrium solid solutions of $(GaAs)_{1-x}Si_x$, *J. Appl. Phys.*, 45, 3690, 1974.
343. **Barnett, S. A., Ray, M. A., Lastras, A., Kramer, B., Greene, J. E., Raccah, P. M., and Abels, L. L.,** Growth and optical properties of single crystal metastable $(GaAs)_{1-x}Ge_x$ alloys, *Electronic Lett.*, 18, 291, 1982.
344. **Cadien, K. C. and Greene, J. E.,** Single phase polycrystalline metastable $(GaSb)_{1-x}Ge_x$ alloys obtained by annealing amorphous mixtures: Ion mixing effects during deposition, *Appl. Phys. Letters*, 40, 329, 1982.
345. **Shah, S. I., Cadien, K. C., and Greene, J. E.,** GaSb-Ge pseudobinary phase diagram, *J. Electronic Materials*, 11, 53, 1982.
346. **Zilko, J. L. and Greene, J. E.,** Growth and phase stability of epitaxial metastable $InSb_{1-x}Bi_x$ films on GaAs. II. Phase stability, *J. Appl. Phys.*, 51, 1560, 1980.
347. **Wood, E. C. E. and Joyce, B. A.,** Tip doping effects in GaAs films grown by molecular beam epitaxy, *J. Appl. Phys.*, 49, 4854, 1978.
348. **Rockett, A., Drummond, T., Greene, J. E., and Morkoc, H.,** Sn segregation in MBE-grown GaAs, *J.* epitaxy, *J. Appl. Phys.*, 49, 4854, 1978.
348. **Rockett, A., Drummond, T., Greene, J. E., and Morkoc, H.,** Surface segregation model for Sn-doped GaAs grown by molecular beam epitaxy, *J. Appl. Phys.*, 53, 7085, 1982.
349. **Krabach, T. N., Wada, N., Klein, M. V., Cadien, K. C., and Greene, J. E.,** Raman scattering from crystalline and amorphous $(GaSb)_{1-x}Ge_x$ semiconducting films, *Solid State Commun.*, in press.
350. **Bajor, G. and Greene, J. E.,** Model calculations for accelerated As ion doping of Si during molecular beam epitaxy, *J. Appl. Phys.*, in press.